Munc13-4 functions as a Ca^{2+} sensor for homotypic secretory granule fusion to generate endosomal exocytic vacuoles

Sang Su Woo, Declan J. James, and Thomas F. J. Martin*
Department of Biochemistry, University of Wisconsin–Madison, Madison, WI 53706

ABSTRACT **Munc13-4 is a Ca^{2+}-dependent SNARE (soluble *N*-ethylmaleimide–sensitive factor attachment protein receptor)- and phospholipid-binding protein that localizes to and primes secretory granules (SGs) for Ca^{2+}-evoked secretion in various secretory cells. Studies in mast cell–like RBL-2H3 cells provide direct evidence that Munc13–4 with its two Ca^{2+}-binding C2 domains functions as a Ca^{2+} sensor for SG exocytosis. Unexpectedly, Ca^{2+} stimulation also generated large (>2.4 µm in diameter) Munc13-4$^+$/Rab7$^+$/Rab11$^+$ endosomal vacuoles. Vacuole generation involved the homotypic fusion of Munc13-4$^+$/Rab7$^+$ SGs, followed by a merge with Rab11$^+$ endosomes, and depended on Ca^{2+} binding to Munc13-4. Munc13-4 promoted the Ca^{2+}-stimulated fusion of VAMP8-containing liposomes with liposomes containing exocytic or endosomal Q-SNAREs and directly interacted with late endosomal SNARE complexes. Thus Munc13-4 is a tethering/priming factor and Ca^{2+} sensor for both heterotypic SG-plasma membrane and homotypic SG-SG fusion. Total internal reflection fluorescence microscopy imaging revealed that vacuoles were exocytic and mediated secretion of β-hexosaminidase and cytokines accompanied by Munc13-4 diffusion onto the plasma membrane. The results provide new molecular insights into the mechanism of multigranular compound exocytosis commonly observed in various secretory cells.**

Monitoring Editor
Patrick J. Brennwald
University of North Carolina

Received: Aug 29, 2016
Revised: Jan 6, 2017
Accepted: Jan 11, 2017

INTRODUCTION

Trafficking of proteins in secretory and endosomal pathways is mediated by fusion machinery comprising soluble *N*-ethylmaleimide–sensitive factor attachment protein receptors (SNAREs), Rab, and SM (Sec 1/Munc18) family proteins acting with a diverse set of tethering/priming factors. R-SNAREs on a vesicle assemble with Q-SNAREs on a recipient compartment in a 1R:3Q ratio to form SNARE complexes that fuse membranes (Jahn and Scheller, 2006; Sudhof and Rothman, 2009; Jahn and Fasshauer, 2012). Multiple factors operate to provide donor-acceptor membrane specificity and compartment-specific fusion. SM proteins regulate SNARE complex assembly (Shen *et al.*, 2007; Ma *et al.*, 2011; Baker *et al.*, 2015) along with pathway-specific tethering/priming proteins (Yu and Hughson, 2010; Ma *et al.*, 2011; James and Martin, 2013; Hong and Lev, 2014). Tethering/priming factors are commonly direct or indirect effectors for Rab GTPases that characteristically reside on specific membranes (Wandinger-Ness and Zerial, 2014). There is little known overlap in the fusion machinery for secretory and endosomal trafficking except for the R-SNAREs VAMP8 and VAMP7, which operate in both secretory granule (SG) exocytosis and endosome fusion in several secretory cell types (Ren *et al.*, 2007; Lorentz *et al.*, 2012; Marshall *et al.*, 2015). Recently the tethering/priming factor Munc13-4 was reported to function in endosome trafficking in addition to its known role in SG exocytosis in hematopoietic secretory cells (Menager *et al.*, 2007; He *et al.*, 2016), but a role for Munc13-4 in Ca^{2+}-triggered endosome fusion has not been characterized.

Membrane fusion events are frequently Ca^{2+} regulated. For regulated SG exocytosis in neuroendocrine cells or synaptic vesicle exocytosis in neurons, C2 domain–containing proteins operate as Ca^{2+} sensors for docking/priming or fusion steps. Synaptotagmin

This article was published online ahead of print in MBoC in Press (http://www.molbiolcell.org/cgi/doi/10.1091/mbc.E16-08-0617) on January 18, 2017.

*Address correspondence to: Thomas F. J. Martin (tfmartin@wisc.edu).

Abbreviations used: CATCHR, complex associated with tethering containing helical rods; EC_{50}, half maximal effective concentration; FWHM, full-width at half-maximum; IL-6, interleukin 6; ILV, intraluminal vesicle; LE, late endosome; RBL, rat basophil leukemia; RE, recycling endosome; SG, secretory granule; SIM, structured illumination microscopy; SNARE, soluble *N*-ethylmaleimide–sensitive factor attachment protein receptor; TIRF, total internal reflection fluorescence; TNF, tumor necrosis factor; VMAT, vesicular monoamine transporter.

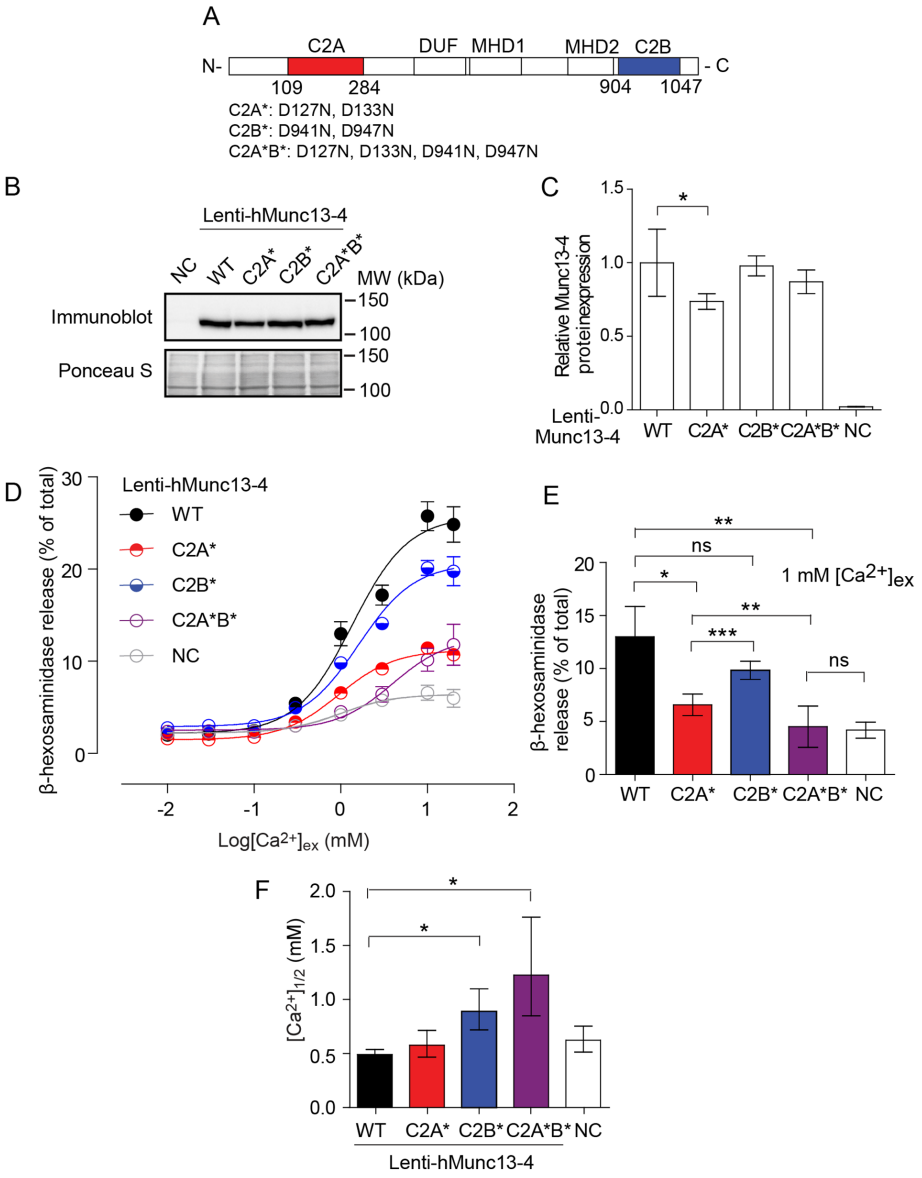

FIGURE 1: Ca^{2+} sensitivity and amplitude of β-hexosaminidase secretion are determined by Munc13-4 C2 domains. (A) Schematic of domain structure of Munc13-4. DUF, domain of unknown function 1041; MHD, Munc13 homology domain. C2A*, C2B*, and C2A*B*, C2 domains with Ca^{2+}-binding mutations. (B) Munc13-4 immunoblotting for rMunc13-4–knockdown cells expressing wild-type (WT) or C2-domain mutant hMunc13-4 proteins. NC, sham infection. Ponceau S stain shows total protein loading of lanes. (C) Quantification of Munc13-4 immunoblotting for knockdown cells expressing WT or C2-domain mutant hMunc13-4 proteins. Band intensities were normalized to the WT Munc13-4 expression. Values are means ± SE ($n = 7$). (D) The Ca^{2+} dose–response for ionomycin-induced β-hexosaminidase secretion in rMunc13-4–knockdown cells expressing WT or C2-domain mutant hMunc13-4 proteins. Values shown are means ± SE ($n = 12$ for WT and $n = 4$ for mutants). Nonlinear fit for WT or mutant Munc13-4 protein expression indicates a Hill coefficient of 1.3 (see *Materials and Methods*). (E) Ionomycin-induced β-hexosaminidase secretion at 1 mM $[Ca^{2+}]_{ex}$ in knockdown cells expressing WT or C2-domain mutant hMunc13-4. Values were extracted from D. (F) EC_{50} values for curves in C plotted as means ± 95% confidence interval.

and Doc2 proteins mediate the Ca^{2+}-triggered fusion of primed SGs or vesicles (Chapman, 2008; Groffen *et al.*, 2010; Pang and Sudhof, 2010; Yao *et al.*, 2011). Upstream of fusion, Munc13-1/2 proteins serve as Ca^{2+} sensors for tethering and priming reactions (Junge *et al.*, 2004; Shin *et al.*, 2010; Lipstein *et al.*, 2012; Imig *et al.*, 2014; Man *et al.*, 2015). For fusion events in endosome trafficking in resting cells, local Ca^{2+} release from luminal sources is considered essential (Hay, 2007; Ghislat and Knecht, 2013), and EF hand–containing proteins are the proposed Ca^{2+} sensors (Colombo *et al.*, 1997; Peters and Mayer, 1998; Pryor *et al.*, 2000; Vergarajauregui *et al.*, 2009; Cao *et al.*, 2015). However, endosome fusion is also regulated by global Ca^{2+} increases in cells (Alvarez de Toledo and Fernandez, 1990; Hartmann *et al.*, 2003; Savina *et al.*, 2005) or in cell-free incubations (Colombo *et al.*, 1997; Holroyd *et al.*, 1999), but it is unclear what Ca^{2+} sensors respond to global Ca^{2+} increases. Global Ca^{2+} increases also induce multigranular compound exocytosis in secretory cells, but the cellular mechanisms responsible for this mode of exocytosis are unknown (Pickett and Edwardson, 2006; Thorn and Gaisano, 2012).

Munc13-4 is a member of a larger Munc13 family of proteins (Koch *et al.*, 2000; Pei *et al.*, 2009). Munc13-4 is a Ca^{2+}-binding, C2 domain–containing protein required for Ca^{2+}-triggered SG exocytosis in cytotoxic T-cells, platelets, neutrophils, mast cells, and endothelial cells (Feldmann *et al.*, 2003; Goishi *et al.*, 2004; Shirakawa *et al.*, 2004; Neeft *et al.*, 2005; Brzezinska *et al.*, 2008; Higashio *et al.*, 2008; Pivot-Pajot *et al.*, 2008; Wood *et al.*, 2009; Ren *et al.*, 2010; Elstak *et al.*, 2011; Zografou *et al.*, 2012; Singh *et al.*, 2013). Munc13-4 deficiency in cytotoxic T-cells results in granules that dock but do not fuse, suggesting Munc13-4's role at a granule-priming step (Feldmann *et al.*, 2003). Munc13-4 mediates SG tethering in rat basophil leukemia (RBL)–2H3 cells, platelets, and neutrophils as a Rab27 effector (Elstak *et al.*, 2011; Johnson *et al.*, 2011; Catz, 2013; Chicka *et al.*, 2016). N-terminal C2A and C-terminal C2B domains of Munc13-4 bracket a region containing Munc13 homology domains that is homologous to complex associated with tethering containing helical rods (CATCHR) domains found in multisubunit tethering complexes (Koch *et al.*, 2000; Feldmann *et al.*, 2003; Neeft *et al.*, 2005; Baker and Hughson, 2016; Figure 1A). We showed that Munc13-4 exhibits Ca^{2+}-dependent exocytic Q-SNARE interactions regulated by Ca^{2+} binding to C2A and Ca^{2+}-dependent phospholipid interactions mediated by Ca^{2+}-binding to C2B (Boswell *et al.*, 2012). Mutations in Ca^{2+}-binding residues abrogated Munc13-4 activity in Ca^{2+}-stimulated, SNARE-dependent liposome fusion and in reconstituting Ca^{2+}-stimulated SG exocytosis in permeable RBL-2H3 cells and platelets (Boswell *et al.*, 2012; Chicka *et al.*, 2016). Such results suggested that Munc13-4 is a Ca^{2+} sensor for a rate-limiting step in SG exocytosis, but this awaits confirmation in intact cells.

The present study identified a requirement for Munc13-4 in Ca^{2+}-dependent SG exocytosis and in Ca^{2+}-triggered endosome fusion in mast cell–like RBL-2H3 cells. Ca^{2+}-dependent SG exocytosis required Ca^{2+}-binding residues in both C2 domains of Munc13-4. Unexpectedly, Ca^{2+} increases also triggered the assembly of large (>2.4 μm in diameter) endosomal vacuoles whose formation depended on Ca^{2+} binding to the C2 domains of Munc13-4. Ca^{2+}-triggered vacuole formation was initiated by the homotypic fusion of Munc13-4$^+$/Rab7$^+$ SGs, followed by fusion with Rab11$^+$ endosomes. Munc13-4$^+$/Rab7$^+$/Rab11$^+$ vacuoles contained diverse cargo (β-hexosaminidase, cytokines) and provided a pathway for the exocytic release of these mediators. The results reveal that multiple membrane fusion events mediate assembly of multigranular compound exocytic organelles and highlight a central role for Munc13-4 in Ca^{2+}-triggered endosome fusion.

RESULTS

Munc13-4 is a Ca^{2+} sensor for Ca^{2+}-evoked degranulation in RBL-2H3 cells

Studies in permeable platelets or RBL-2H3 cells and in reconstituted SNARE-dependent liposome fusion assays suggested that Munc13-4 functions as a Ca^{2+} sensor for SG exocytosis (Ren *et al.*, 2010; Boswell *et al.*, 2012). To assess whether Munc13-4 functions as a Ca^{2+} sensor in mast cell–like RBL-2H3 cells (Seldin *et al.*, 1985), we conducted studies in Munc13-4–deficient cell lines established by stably expressing a lentiviral rat(r) Munc13-4 short hairpin RNA (shRNA; Supplemental Figure S1A). rMunc13-4–deficient cells were used to express Ca^{2+}-binding mutants of human(h) Munc13-4 harboring two D-to-N substitutions in C2 domains (C2A*, C2B*, and C2A*B*; Figure 1A). Similar replacement studies with synaptotagmin-1 or Doc2 provided evidence for a Ca^{2+} sensor role of these proteins in synaptic vesicle exocytosis because mutations shifted the Ca^{2+} sensitivity of secretion (Groffen *et al.*, 2010; Yao *et al.*, 2011; Sudhof, 2012). rMunc13-4 depletion reduced ionomycin-stimulated β-hexosaminidase secretion by 70% compared with control cells (Supplemental Figure S1B), as previously found (Elstak *et al.*, 2011). Stimulated β-hexosaminidase secretion was restored by the expression of wild-type hMunc13-4, which evades the shRNA for rMunc13-4 (Supplemental Figure S1B). We optimized expression of wild-type and mutant hMunc13-4 proteins to be comparable (Figure 1, B and C) because pilot studies found a nonlinear relationship between hMunc13-4 protein expression and secretory responses. Each hMunc13-4 mutant protein partially restored stimulated β-hexosaminidase secretion but with altered characteristics (Figure 1D). Maximal secretion at 10 mM $[Ca^{2+}]_{ex}$ was reduced for C2A* and C2A*B* proteins compared with wild-type protein, indicating decreased efficacy. Thus the C2A domain, reported to regulate Ca^{2+}-stimulated SNARE binding (Boswell *et al.*, 2012), controlled response amplitude. At 1 mM $[Ca^{2+}]_{ex}$, C2A* and C2B* proteins were partially active, whereas C2A*B* was inactive, indicating additive loss of function for each mutant C2 domain (Figure 1E). Half-maximal effective $[Ca^{2+}]_{ex1/2}$ values were similar for C2A* and wild-type proteins (0.58 and 0.49 mM, respectively) whereas C2B* and C2A*B* exhibited increased values (0.89 and 1.23 mM, respectively; Figure 1F). Thus the C2B domain, reported to mediate Ca^{2+}-dependent phospholipid binding (Boswell *et al.*, 2012; Chicka *et al.*, 2016), conferred overall Ca^{2+} sensitivity. Combined mutations in C2A*B* affected response amplitude and Ca^{2+} sensitivity (Figure 1, D and F). The results indicate that Munc13-4 functions as a Ca^{2+} sensor for SG exocytosis, integrating the Ca^{2+}-dependent functions of both C2 domains, similar to in vitro findings (Boswell *et al.*, 2012).

Munc13-4$^+$ SGs form enlarged vacuoles upon ionomycin stimulation

Expressed fluorescent constructs of Munc13-4 localize to SGs in RBL-2H3 cells (Neeft *et al.*, 2005; Higashio *et al.*, 2008). We extended this to endogenous Munc13-4 in immunofluorescence studies in which Munc13-4 colocalized with vesicular monoamine transporter 2 (VMAT2; Figure 2A), the SG monoamine transporter. Munc13-4 immunofluorescence was not detected in Munc13-4–knockdown cells (Supplemental Figure S2A). Ionomycin treatment for 20 min markedly altered the localization of both Munc13-4 and VMAT2. There was extensive loss of SGs as expected for stimulated cells, but, unexpectedly, there was also the formation of large (>2.4 μm in diameter) vacuoles in which Munc13-4 and VMAT2 colocalized (Figure 2A). VMAT2 is membrane integrated, and so it is likely that a subset of SGs engaged in homotypic fusion to generate vacuoles. We further characterized membrane components on vacuoles to determine possible fusion events responsible for vacuole formation. SGs in RBL-2H3 and other hematopoietic cells acquire endosomal properties and represent a subset of Rab7$^+$ late endosomes (LEs; Vincent-Schneider *et al.*, 2001; Cohen *et al.*, 2012; Luzio *et al.*, 2014; Azouz *et al.*, 2014b). Rab7 colocalized with Munc13-4 on SGs in resting cells, as expected (Azouz *et al.*, 2012), and ionomycin treatment increased Rab7 colocalization with Munc13-4 on large vacuoles, suggesting that SGs may also fuse with additional Rab7$^+$ LEs (Figure 2, B and C). This was also suggested by studies showing that vacuoles were LAMP2$^+$ (Supplemental Figure S2B). Rab11, corresponding to recycling endosomes (REs), did not significantly colocalize with Munc13-4 in resting cells but localized to vacuoles with Munc13-4 in ionomycin-treated cells (Figure 2, B and C), indicating that REs participate in vacuole generation. Rab5, corresponding to early endosomes, did not significantly colocalize with Munc13-4 in resting or stimulated cells (Figure 2, B and C). The results suggest that Ca^{2+}-induced vacuoles result from a merge of Munc13-4$^+$/Rab7$^+$ SGs with Rab11$^+$ REs and with additional Rab7$^+$ LEs.

We assessed the apparent merge of Munc13-4$^+$ membranes with Rab7$^+$ and Rab11$^+$ membranes by high-resolution (~100 nm) structured illumination microscopy (SIM; Figure 2D). Munc13-4 colocalized with Rab7 and Rab11 on the vacuole in stimulated cells, indicating residence in a common membrane (Figure 2D, inset slices). High-pressure freezing/freeze-substitution electron microscopy (Murk *et al.*, 2003) revealed that the vacuole was a single membrane-enclosed structure containing numerous 30- to 200-nm intraluminal vesicles (ILVs; Figure 2E). This indicated that vacuoles were enlarged multivesicular bodies similar to the Rab11$^+$ vacuoles described for ionophore-treated erythroleukemia cells (Savina *et al.*, 2005). SGs in RBL-2H3 cells contain ILVs (Vincent-Schneider *et al.*, 2001), consistent with vacuole generation involving homotypic SG fusion.

We also assessed the distribution of R-SNAREs that might function in vacuole formation (Supplemental Figure S3, A and B). VAMP8 is a LE R-SNARE that mediates SG exocytic fusion in hematopoietic secretory cells (Paumet *et al.*, 2000; Lippert *et al.*, 2007; Ren *et al.*, 2007; Lorentz *et al.*, 2012). A fraction of VAMP8 colocalized with Munc13-4 on SGs in resting RBL-2H3 cells and also on the vacuole in Ca^{2+}-stimulated cells. VAMP3, an R-SNARE on RE membranes (Lorentz *et al.*, 2012), was widely distributed in the cytoplasm, and its fluorescence occasionally overlapped with that of Munc13-4 in resting cells. VAMP3 did appear to colocalize with Munc13-4 on the vacuole membrane in Ca^{2+}-stimulated cells, consistent with fusion with Rab11$^+$ REs in vacuole generation. By contrast, VAMP7 appeared to localize within the vacuole possibly associated with ILVs. Overall the results were consistent with

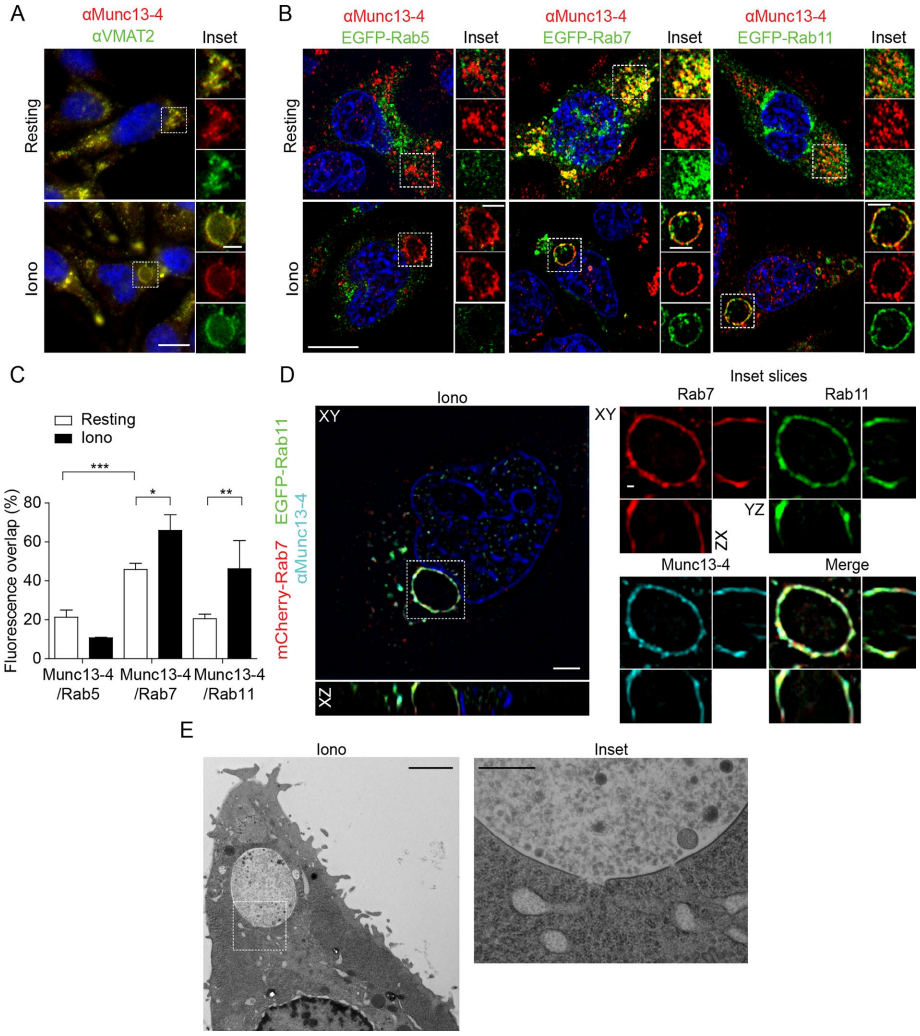

FIGURE 2: Localization of Munc13-4, VMAT2, and endosomal Rab GTPases. (A) Immunofluorescence for Munc13-4 (red) and VMAT2 (green) in resting and ionomycin-stimulated cells. Nuclei pseudocolored in blue are Hoechst stained. Images were acquired by epifluorescence illumination and deconvolved. (B) Immunofluorescence for Munc13-4 compared with EGFP-Rab5, 7, or 11 in resting and ionomycin-stimulated cells. Rab7 and Rab11, but not Rab5, colocalized with Munc13-4 on vacuoles in ionomycin-stimulated cells. Images are single optical sections acquired by confocal microscopy and deconvolved. Scale bars, 10 μm (whole cells), 3 μm (insets). (C) Colocalization of Munc13-4 with Rab GTPases in resting and ionomycin-treated cells was quantitated by Manders' overlap coefficient. Values shown are percentage of Munc13-4$^+$/Rab$^+$ pixels of total Rab$^+$ pixels (see *Materials and Methods*). Bars are means ± SE (n = 3–9). (D) mCherry-Rab7 (red)– and EGFP-Rab11 (green)–expressing cells were treated with ionomycin and fixed for Munc13-4 immunostaining (light blue) and Hoechst staining (dark blue). A representative vacuole was imaged by 3D SIM. Whole-cell images are equatorial and vertical sections in a 3D stack along *XY*- and *XZ*-planes. Insets, equatorial and vertical sections along *XY*-, *YZ*-, and *XZ*-planes in each channel color. Scale bars, 3 μm (whole cells), 0.5 μm (inset slices). (E) Morphology of a representative vacuole in ionomycin-treated cell imaged by transmission electron microscopy. The dark half-circle at the bottom is a nucleus. Scale bars, 2 μm (whole cell), 0.5 μm (inset).

vacuole formation resulting from fusion between SG, LE, and RE membranes.

Munc13-4 is required for Ca^{2+}-triggered vacuole formation

Localization to the vacuole membrane suggested that Munc13-4 participates in one or more of the Ca^{2+}-induced membrane fusion events that lead to vacuole formation. We determined whether Munc13-4 was required for vacuole formation using Munc13-4–knockdown RBL-2H3 cells. Rab27 directly binds Munc13-4, and this complex positively regulates mast cell and platelet degranulation (Goishi *et al.*, 2004; Shirakawa *et al.*, 2004; Elstak *et al.*, 2011; Singh *et al.*, 2013). Endogenous Rab27b colocalized with Munc13-4 on SGs in resting wild-type RBL-2H3 cells (Neeft *et al.*, 2005) and was present on the vacuole in ionomycin-treated cells (Supplemental Figure S3, C and D). Thus we quantified vacuole formation by measuring the surface area of Rab27b$^+$ vesicles (Figure 3, A and B). The largest Rab27b$^+$ vesicles in resting wild-type cells had a mean area of 1.94 ± 1.25 μm^2 (±SD), whereas 20-min ionomycin treatment increased this to 4.05 ± 3.39 μm^2 (Figure 3B). Twenty-five percent of ionomycin-treated wild-type cells exhibited at least one vacuole larger than the size threshold (see legend to Figure 3B), ranging from 5 to 14 μm^2. By contrast, ionomycin treatment of Munc13-4–knockdown cells failed to stimulate vacuole formation (Figure 3, A–C, and Supplemental Figure S3E). Expression of hMunc13-4 in the knockdown cells restored vacuole formation to a level similar to that in wild-type cells (Figure 3C and Supplemental Figure S3E). Alternatively, we detected vacuole formation by the localization of enhanced green fluorescent protein (EGFP)–Rab11$^+$ with mCherry-Rab7$^+$ on vacuoles in ionomycin-treated cells (Figure 3D). The knockdown of Munc13-4 eliminated vacuole formation (Figure 3, D and E), confirming that Munc13-4 is essential for Ca^{2+}-induced vacuole formation.

Ionomycin treatment in RBL-2H3 cells elevates cytoplasmic Ca^{2+} to levels similar to those with IgE receptor activation, although the latter elicits Ca^{2+} oscillations (Lin and Gilfillan, 1992; Lee and Oliver, 1995). We determined whether vacuole formation also occurs under physiological stimulation conditions of immunoglobulin E (IgE) receptor activation. The formation of Rab7$^+$/Rab11$^+$ vacuoles occurred with IgE-sensitized cells stimulated by antigen but not with IgE alone (Figure 3, F and G, and Supplemental Figure S3F). Similarly, treatment with thapsigargin to mobilize intracellular stored Ca^{2+} induced vacuole formation (Figure 3, F and G, and Supplemental Figure S3G). Similar-sized vacuoles were generated by each stimulus (Figure 3G), but the frequency of vacuole occurrence differed (Figure 3F). The results suggest that the frequency of vacuole formation depends on the magnitude and persistence of $[Ca^{2+}]_i$ increases achieved for each stimulus (Lin and Gilfillan, 1992; Lee and Oliver, 1995). These studies indicate that Ca^{2+}-induced vacuole formation occurs under physiological stimulation conditions.

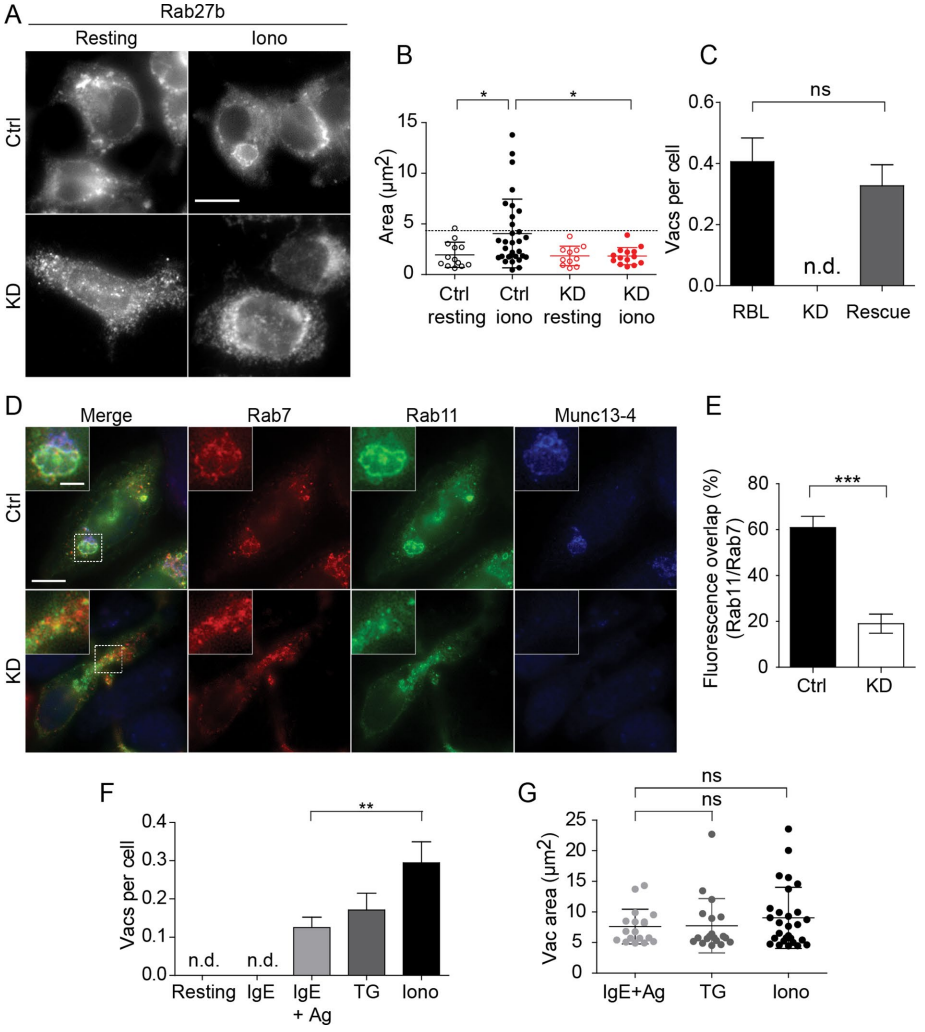

FIGURE 3: Ca^{2+}-induced vacuole formation depends on Munc13-4. (A) Immunofluorescence of Rab27b in control or Munc13-4 knockdown (KD) cells under resting or ionomycin-stimulated conditions. (B) Profile area of largest $Rab27b^+$ vacuoles per cell shown as mean ± SD (n = 13, 35, 11, 15). Dotted line indicates a threshold value assigned as the mean area for control cells +2 SD (4.4 μm²). (C) Frequency of vacuole (Vac) formation in control (RBL) or Munc13-4 KD cells infected or not with lenti-hMunc13-4 (Rescue). Cells were stimulated with ionomycin, and vacuoles larger than the threshold 4.4 μm² were registered and normalized by cell number. Values are means ± SE (n = 101, 93, 101). n.d., none detected. See Supplemental Figure S3, E and D. Localization of mCherry-Rab7, EGFP-Rab11, and immunoreactive Munc13-4 in ionomycin-treated control (top) and Munc13-4 KD (bottom) cells. (E) Fluorescence overlap analysis between Rab7 and Rab11 in Munc13-4 KD cells from D by Manders' overlap coefficient. Values indicate percentage of $Rab11^+/Rab7^+$ pixels of total $Rab7^+$ pixels and are mean ± SE (n = 6). (F) Frequency of vacuole (Vacs) formation induced by 20-min treatments with IgE, IgE with DNP antigen, thapsigargin (TG), or ionomycin (iono). Values are means ± SE (n = 102, 122, 144, 111, 112). See Supplemental Figures S3, F and G. (G) Size of vacuoles induced by different stimuli used in F. Images were acquired by epifluorescence illumination and deconvolved. Scale bars, 10 μm (whole cells), 3 μm (insets).

Munc13-4 is required for vacuole formation involving Ca^{2+}-dependent homotypic fusion of SGs

The preceding established that Munc13-4 was essential for Ca^{2+}-induced vacuole formation but did not determine which membrane fusion steps depended on Munc13-4. Live-cell imaging studies were used to resolve sequential fusion events in vacuole formation in ionomycin-treated cells (Figure 4A and Supplemental Video S1). $Rab7^+$ SGs began forming a vacuole within 2 min after ionomycin stimulation in the cell shown (Figure 4A, inset, arrow). Subsequently $Rab11^+$ REs merged with the $Rab7^+$ vacuoles, with vacuole formation complete by 5–6 min in this example (Figure 4A, inset, merge). A delayed recruitment of Rab11 to $Rab7^+$ vacuoles was reproducibly observed (Figure 4C), indicating that $Rab7^+$ vacuoles form first and serve as acceptors for $Rab11^+$ endosomes. We conducted similar studies to detect the merge of $Rab11^+$ endosomes with assembling Munc13-4$^+$ vacuoles (Figure 4B) and found a similar delay for the recruitment of $Rab11^+$ endosomes to the forming vacuole (Figure 4C).

Similar studies in Munc13-4–knockdown cells were conducted to detect the merge of $Rab11^+$ endosomes with $Rab7^+$ vacuoles, but we found that $Rab7^+$ vacuoles failed to form (Figure 4D and Supplemental Video S2). $Rab7^+$ structures remained constant in size over a 15-min ionomycin stimulation period in the absence of Munc13-4 (Figure 4E). This indicated that Munc13-4 was required for an early step in $Rab7^+$ vacuole formation. Because a subset of $Rab7^+$ LEs are Munc13-4$^+$ SGs, we determined whether the earlier step in vacuole formation involves the homotypic fusion of $Rab7^+$/Munc13-4$^+$ SGs. Coexpressed mKate2-Munc13-4 and EGFP-Rab7 colocalized to SGs (Figure 5A, left), and ionomycin treatment promoted robust formation of Munc13-4$^+$/$Rab7^+$ vacuoles (Figure 5A, right and inset, and Supplemental Video S3). Compared to Rab27b immunofluorescence for control cells, there was an increased number of vacuoles in some Munc13-4/Rab7–overexpressing cells compared with wild-type cells, but this was variable and not significant (Figure 5B). Overall these studies suggest that the Munc13-4–dependent step for Ca^{2+}-stimulated vacuole formation consists of the homotypic fusion of Munc13-4$^+$/$Rab7^+$ SGs to form Munc13-4$^+$/$Rab7^+$ vacuoles.

We determined whether Ca^{2+} binding to Munc13-4 was essential for vacuole formation. rMunc13-4–knockdown cells failed to form $Rab27b^+$ vacuoles in response to ionomycin stimulation, whereas expression of hMunc13-4 fully rescued vacuole formation (Figure 5, C and D). By contrast, expression of the C2A*B* hMunc13-4 mutant failed to rescue vacuole formation. Similarly, cooverexpression of EGFP-Rab7 and mKate2-hMunc13-4 rescued vacuole formation in rMunc13-4–knockdown cells (Figure 5E, top), whereas cooverexpression of EGFP-Rab7 and mKate2-C2A*B* hMunc13-4 failed to rescue (Figure 5E, bottom), as quantitated in Figure 5F. These results indicate that Munc13-4 requires Ca^{2+} binding for its role in vacuole formation. Collectively, the studies of Figures 4 and 5 indicate that Munc13-4 functions in Ca^{2+}-triggered vacuole formation at the homotypic fusion of Munc13-4$^+$/$Rab7^+$ SGs to form Munc13-4$^+$/$Rab7^+$ vacuoles, and these intermediates fuse with $Rab11^+$ REs to form mature vacuoles (Figure 5G). Munc13-4 may

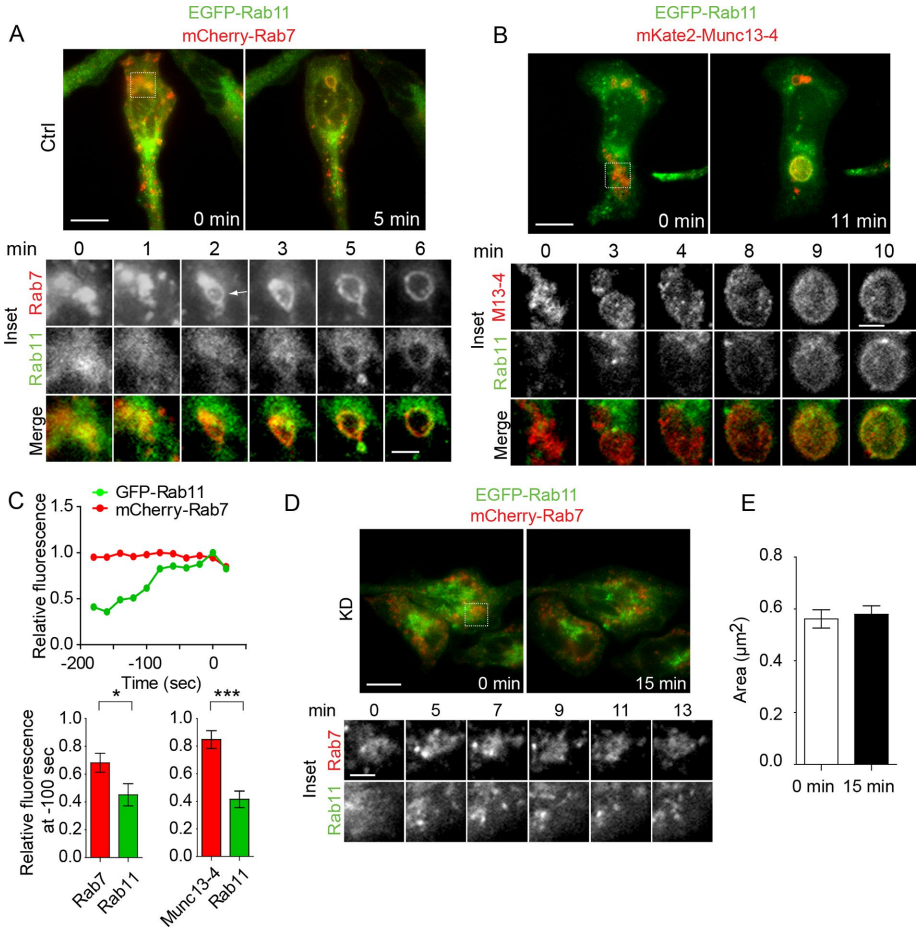

FIGURE 4: Munc13-4-dependent vacuole formation resolved by epifluorescence time-lapse imaging. (A) Vacuole formation in ionomycin-treated cells visualized with EGFP-Rab11 (green) and mCherry-Rab7 (red). Arrow in inset indicates formation of Rab7$^+$ vacuole intermediate. Vacuole formation was variable with Rab11$^+$/Rab7$^+$ vacuoles, generally forming in 8.9 ± 4.2 min after ionomycin stimulation and persisting for up to ~60 min (see Figure 7). In this representative set of images, Rab11 was recruited after formation of Rab7$^+$ vacuole (see C). (B) Vacuole formation in cells expressing EGFP-Rab11 (green) and mKate2-Munc13-4 (red) after ionomycin stimulation. The appearance of Rab11 on the vacuole followed that of Munc13-4 (see C). (C) Delayed recruitment of Rab11 onto vacuoles. ROIs were drawn on vacuole membrane, and mean intensity was measured for green and red channels at each acquisition time. Top, relative intensity change of mCherry-Rab7 (red) and GFP-Rab11 (green) during vacuole formation. The 0-s mark indicates the time point of peak Rab11 intensity on vacuoles. Bottom, relative intensity of fluorescence probes on vacuole at −100 s. Bars indicate mean ± SE (Rab7-Rab11 pair, $n = 11$; Munc13-4-Rab11 pair, $n = 6$). (D) Vacuoles failed to form in similar studies with Munc13-4 KD cells, in which Rab7$^+$ vacuole intermediates were not observed. (E) Profile area of Rab7$^+$ vesicles before and after ionomycin treatment in Munc13-4 KD cells. Mean values ± SE ($n = 246$ vesicles before and $n = 245$ vesicles after stimulation in four cells) are shown and were not different before and after ionomycin treatment. Images were acquired by epifluorescence illumination and deconvolved. Scale bars,10 μm (whole cells), 3 μm (insets).

function in other membrane fusion events beyond homotypic SG fusion, but the absence of Rab7$^+$ vacuole intermediates in Munc13-4 knockdown cells precluded determination of whether Munc13-4 is also required for the merge of Rab11$^+$ REs with vacuoles.

Munc13-4 promotes liposome fusion with late endosomal SNAREs

The preceding indicated that Munc13-4 and its Ca^{2+}-binding C2 domains are required for SG exocytosis and for endosomal vacuole formation in Ca^{2+}-stimulated RBL-2H3 cells. These fusion events may be mediated by VAMP8 on the SG membrane (Supplemental Figure S3, A and B; Paumet *et al.*, 2000; Puri and Roche, 2008; Tiwari *et al.*, 2008). For SG exocytosis, VAMP8 was reported to pair with syntaxin-4 and SNAP-23 (Paumet *et al.*, 2000; Woska and Gillespie, 2011; Lorentz *et al.*, 2012; Wesolowski and Paumet, 2014), and we found that Ca^{2+}-activated Munc13-4 accelerates the fusion of liposomes containing VAMP8 with liposomes containing syntaxin-1/SNAP-25, the neuronal homologues of syntaxin-4/SNAP-23 (Figure 6B). The Munc13-4–stimulated FRET between liposomes was strictly dependent on Ca^{2+} (Figure 6B) and on the R- and Q-SNARE proteins (Figure 6C).

By contrast, homotypic LE fusion was reported to use VAMP8 paired with syntaxin-7, Vti1b, and syntaxin-8 (Antonin *et al.*, 2000, 2002; Luzio *et al.*, 2009). We found that Munc13-4 strongly promoted the fusion of VAMP8-containing liposomes with LE Q-SNARE (syntaxin-7, Vti1b, syntaxin-8) liposomes in the presence of Ca^{2+} (Figure 6A). No effects of Munc13-4 or Ca^{2+} were observed with liposomes lacking SNAREs (Figure 6C). Munc13-4 exhibited strongly Ca^{2+}-dependent binding to the Q-SNARE liposomes but did not bind liposomes lacking SNARE proteins (Figure 6, E and F). The Ca^{2+}-dependent binding of Munc13-4 was also observed for liposomes containing Vti1b alone but not to liposomes containing syntaxin-7 or syntaxin-8 (Figure 6, D and F; see *Discussion*). Although the fusion of liposomes reconstituted with LE SNAREs has previously been described (Shen *et al.*, 2007; Yu *et al.*, 2013), Ca^{2+}-bound Munc13-4 is the first regulatory factor identified that stimulates liposome fusion with reconstituted mammalian LE SNAREs. The results suggest that Munc13-4 could act as a Ca^{2+} sensor on membranes that contain LE SNARE proteins.

The association of Munc13-4 with LE SNARE complexes was confirmed by immunoprecipitation studies in RBL-2H3 cells expressing GFP-Munc13-4, which localizes normally to membranes (Figure 4). Immunoprecipitation of GFP-Munc13-4 by GFP-Trap nanobodies was highly efficient (Figure 6Ga) and found to coisolate syntaxin-7, Vti1b, syntaxin-8, and VAMP8 (Figure 6G, b–e). The retention of LE SNAREs by GFP-Munc13-4 was in each case enhanced by Ca^{2+} addition to the lysates. Each of the Munc13-4-associated LE SNARE proteins was isolated as ~50-kDa or higher–molecular weight (MW) complexes that consisted of homooligomers or heterooligomers (Figure 6 legend). We recapitulated these homooligomers or heterooligomers in our SDS–PAGE system by assembling purified LE SNARE proteins into heterotetrameric complexes that were subject to nonboiling and boiling SDS conditions shown for Vti1b (Figure 6H). These studies identifying ~50-kDa or higher-MW LE SNARE complexes confirmed and extended

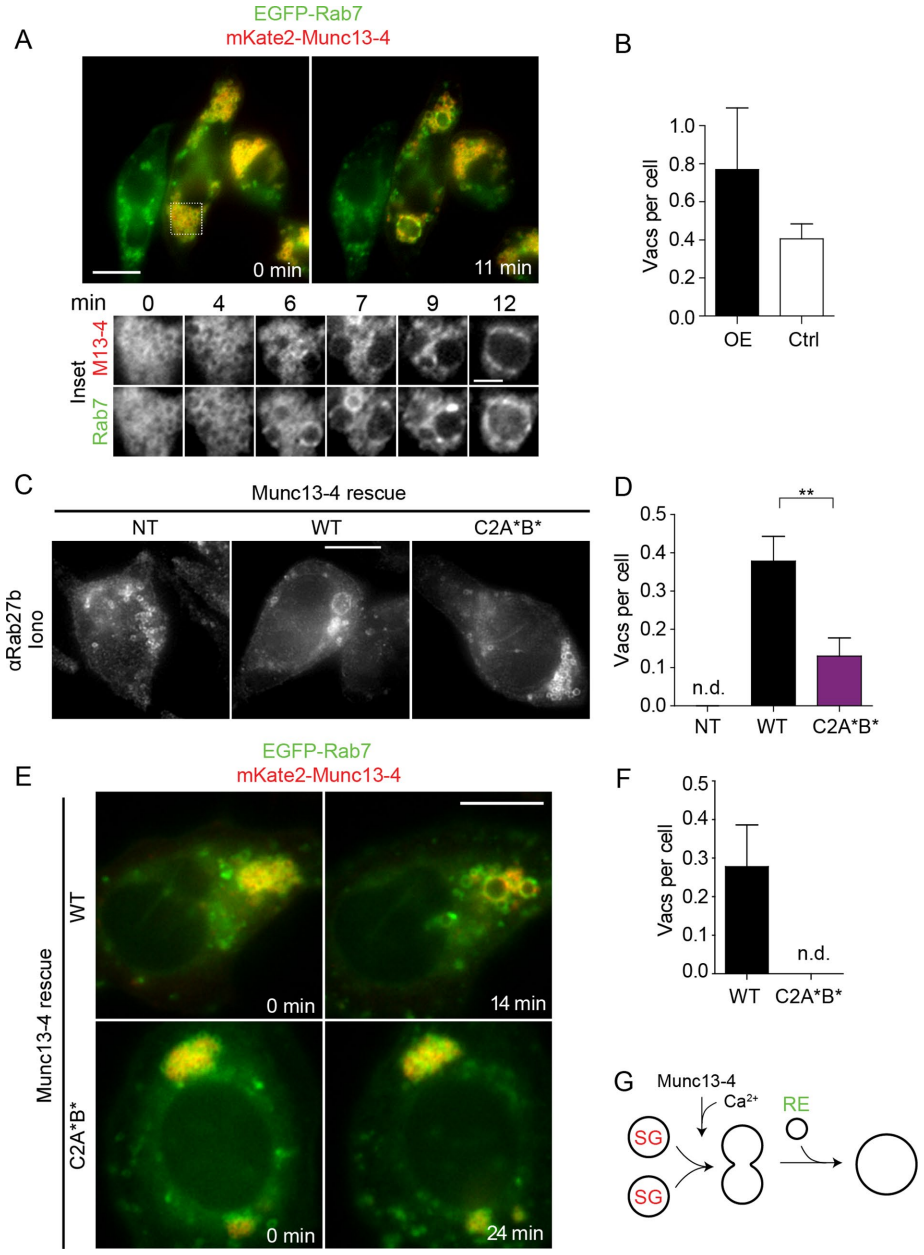

FIGURE 5: Vacuole formation involves homotypic SG fusion and requires Ca^{2+} binding to Munc13-4. (A) Vacuole formation in ionomycin-treated cells overexpressing mKate2-Munc13-4 (red) and EGFP-Rab7 (green). Insets, time course of Munc13-4$^+$/Rab7$^+$ vacuole formation. (B) Frequency of vacuole (Vacs) formation in ionomycin-treated cells that express mKate2-Munc13-4 and EGFP-Rab7 (OE) in comparison to cells with endogenous expression level (control [Ctrl]). Control values are from Figure 3C. Values are means ± SE (OE, $n = 13$; Ctrl, $n = 101$). Some overexpressing cells exhibited more vacuoles than control, but there was no significant difference in the mean number. (C) Dependence of vacuole formation on Ca^{2+} binding to Munc13-4. Vacuole formation detected by Rab27b immunofluorescence in ionomycin-stimulated KD cells expressing WT or C2A*B* mutant hMunc13-4 (NT, nontransduced). (D) Frequency of vacuole (Vacs) formation quantitated in experiments similar to that of C. Values are means ± SE ($n = 112$, 148, 123). n.d., none detected. (E) Munc13-4 is a Ca^{2+} sensor for homotypic SG fusion. Vacuole formation monitored by live-cell imaging for KD cells expressing WT or C2A*B* hMunc13-4. SGs in cells expressing C2A*B* Munc13-4 failed to fuse with each other in comparison to SGs in cells expressing WT hMunc13-4. (F) Frequency of vacuoles (Vacs) in studies similar to that of E. Values are means ± SE ($n = 8$); n.d., none detected. (G) Route for vacuole formation involving fusion of Rab7$^+$ SGs followed by fusion with Rab11$^+$ endosomes. Images were acquired by epifluorescence illumination and deconvolved. Scale bars, 10 μm (whole cells), 3 μm (insets).

the previous findings (Mascia and Langosch, 2007) that specific full-length LE SNARE proteins form very stable associations with one another (see *Discussion*). We conclude that Munc13-4 preferentially associates with or stabilizes LE SNARE complexes from RBL-2H3 cells.

Ca^{2+}-induced vacuoles are exocytic

We addressed the physiological role of the Ca^{2+}-induced vacuole. Mature vacuoles are of mixed endosomal origin (Rab7$^+$, Rab11$^+$, ILV$^+$, LAMP2$^+$) and contain SG constituents (Rab27b$^+$, Munc13-4$^+$, VMAT2$^+$, β-hexosaminidase$^+$). Ionomycin-stimulated β-hexosaminidase release extends over the time period of vacuole assembly, consistent with a possible exocytic role for the vacuole (Supplemental Figure S5A). This was confirmed in live-cell studies by coexpression of β-hexosaminidase (Hexβ)–mCherry with EGFP-Munc13-4 (Figure 7A). Hexβ-mCherry localized to the lumen of a subpopulation of Munc13-4$^+$ SGs in resting cells (Figure 7A, insets). Some Munc13-4$^+$ SGs fused with each other upon ionomycin treatment to form a vacuole with Hexβ-mCherry content (Supplemental Video S4). Hexβ-mCherry content suddenly disappeared from the lumen of mature vacuoles within a 1-min frame, suggesting that exocytosis occurred (e.g., Figure 7A, inset 3, 18–19 min). Unit-size SGs (full-width at half-maximum [FWHM] ≈ 0.75 μm; Figure 7A, inset 1, arrow; Grimberg *et al.*, 2003) and intermediate-size vacuoles (FWHM ≈ 1.35 μm; Figure 7A, inset 2, arrowhead) also suddenly lost Hexβ-mCherry content in ionomycin-treated cells. Exocytosis from structures of various sizes is a type of Ca^{2+}-triggered compound exocytosis termed multigranular, in which SGs merge with one another before their fusion with the plasma membrane (Alvarez de Toledo and Fernandez, 1990; Hartmann *et al.*, 2003; Dvorak, 2005). It is noteworthy that vacuoles also fused with vacuoles that had undergone exocytosis (Figure 7A, inset 4), which is another form of compound exocytosis, termed sequential exocytosis (Nemoto *et al.*, 2001; Behrendorff *et al.*, 2011).

Simultaneous epifluorescence and total internal reflection fluorescence (TIRF) microscopy imaging confirmed that vacuoles underwent exocytosis (Figure 7B and Supplemental Videos S4 and S5). In the example shown, two large vacuoles containing Hexβ-mCherry were evident; one of these contacted the plasma membrane during the interval (44–48 min) shown. Contact of the vacuole with the plasma membrane was

evident at 45 min by the focal brightening of EGFP-Munc13-4 in TIRF (Figure 7B, bottom). Hexβ-mCherry was released in the next frame (Figure 7B, top). EGFP-Munc13-4 darkened at the focal contact (Figure 7B, bottom) at 46 min, corresponding to fusion pore formation, and subsequently spread by diffusion onto the plasma membrane. The apparent fusion pore diameter was >500 nm and lasted for >1 min. Thus large vacuoles dock onto the plasma membrane, form a fusion pore, discharge contents, and deliver the vacuole membrane constituent Munc13-4 onto the plasma membrane. The exocytosis of a smaller vacuole (FWHM ≈ 1.2 μm) was analyzed by TIRF at a higher frame rate to measure the diffusion of Munc13-4 onto the plasma membrane (Figure 7C and Supplemental Video S6). The vacuole approached the plasma membrane (4.8–8 s), docked (12.8–33.6 s), and opened a fusion pore at ~36 s. The diffusion coefficient for the lateral spread of EGFP-Munc13-4 of ~0.07 $\mu m^2/s$ (Supplemental Figure S5, B and C) was slower than lipid diffusion (~1 $\mu m^2/s$) but only approximately threefold slower than VAMP2-EGFP diffusion in the exocytosis of smaller (~0.3 μm in diameter) SGs in chromaffin cells (~0.2 $\mu m^2/s$; Allersma *et al.*, 2004). The results indicate that Munc13-4 retains its membrane association before, during, and after fusion as it diffuses from the vacuole membrane onto the plasma membrane.

Ca^{2+}-induced vacuoles release multiple contents

Mature vacuoles were characterized as $Rab11^+$ and might receive cargo from the Golgi by the fusion of Rab11 endosomes. Cytokine trafficking in macrophages, specifically that of tumor necrosis factor α (TNFα) and IL-6, was reported to be mediated by $Rab11^+$ endosomes (Manderson *et al.*, 2007). We confirmed possible post-Golgi cytokine trafficking in $Rab11^+$ endosomes for RBL-2H3 cells at early times after expression of TNFα–yellow fluorescent protein (YFP) with CFP-Rab11 or IL-6–mCherry with EGFP-Rab11, where significant colocalization in perinuclear regions was observed (Figure 8A). $Munc13\text{-}4^+$ vacuoles formed after ionomycin stimulation were found to contain TNFα-YFP (Figure 8B) and IL-6–mCherry (Figure 8C). In both cases, these cargoes disappeared from vacuoles during exocytosis (marked as 0 s in Figure 8, B and C). The results indicate that cytokines represent additional cargo that can be packaged into vacuoles and discharged from them upon exocytosis.

DISCUSSION

Munc13-4 is a Ca^{2+}-dependent SNARE- and phospholipid-binding protein that localizes to SGs in resting mast cells. The present work broadens Munc13-4's cellular role as a tethering/priming factor for SG exocytosis to endosomal fusion events. With its Ca^{2+}-binding C2 domains, Munc13-4 functions as a Ca^{2+} sensor for heterotypic fusion events (SG exocytosis) and for homotypic fusion events (SG-SG fusion). The latter leads to the de novo assembly of endosomal vacuoles of complex composition that correspond to multigranular compound organelles. The endosomal vacuoles are exocytic, leading to the externalization of diverse cargo, including lysosomal enzymes and cytokines. Munc13-4 is the first example of a dual-function tethering/priming factor that operates in both SG exocytosis and homotypic SG fusion. This provides new insights into mechanisms underlying Ca^{2+}-triggered multigranular compound exocytosis.

Ca^{2+} sensor roles of Munc13-4 for multiple membrane fusion events

Ca^{2+}-dependent SG exocytosis involves multiple steps, including SG translocation to the plasma membrane with subsequent docking, priming, and fusion steps. Each step in the pathway may involve Ca^{2+}-dependent regulators that serve as Ca^{2+} sensors. Munc13-4 is proposed to function in the priming of SGs for fusion (Feldmann *et al.*, 2003) or in the tethering or docking of SGs at the plasma membrane (Elstak *et al.*, 2011; Johnson *et al.*, 2011; Chicka *et al.*, 2016) in secretory cells of hematopoietic lineage. We and others found that Ca^{2+}-binding mutations in the C2 domains of Munc13-4 inhibited the Ca^{2+}-dependent fusion of liposomes containing exocytic SNARE proteins (Boswell *et al.*, 2012; Chicka *et al.*, 2016). These studies suggested that Munc13-4 might function as a Ca^{2+} sensor in SG exocytosis. We provide direct evidence for this in intact cells by finding that the C2A* and C2B* mutant Munc13-4 proteins altered the amplitude and Ca^{2+} sensitivity of Ca^{2+}-induced β-hexosaminidase release, respectively. The role of both C2 domains was indicated by an additive loss of function for C2A*2B* Munc13-4. $Munc13\text{-}4^+$ SGs were not tethered or docked at the plasma membrane in RBL-2H3 cells in our studies but translocated to the plasma membrane in Ca^{2+}-stimulated cells. We suggest that Munc13-4 localized on SGs could tether SGs to the plasma membrane in stimulated cells via Ca^{2+}-dependent C2B interactions with acidic phospholipids (Boswell *et al.*, 2012; Chicka *et al.*, 2016). Ca^{2+} binding to C2 domains could also unmask SNARE-binding sites on Munc13-4 to initiate SNARE complex assembly for docking and priming SGs (Boswell *et al.*, 2012; He *et al.*, 2016).

Remarkably, Munc13-4 also functioned as a Ca^{2+} sensor to promote the de novo, Ca^{2+}-triggered assembly of an endosomal vacuole. The SGs in RBL-2H3 cells and other hematopoietic cells acquire late endosomal properties and are $Rab7^+$ (Vincent-Schneider *et al.*, 2001; Benado *et al.*, 2009; Cohen *et al.*, 2012; Azouz *et al.*, 2014a; Luzio *et al.*, 2014). We found that Ca^{2+}-activated Munc13-4 promoted the homotypic fusion of SGs to form $Rab27b^+/Rab7^+/Munc13\text{-}4^+/VMAT2^+/β\text{-}hexosaminidase^+/ILV^+$ vacuolar intermediates. Vacuoles increase in size as they mature and become $Rab11^+$ from a late fusion with REs (Figure 9). Studies in cytotoxic T-cells suggested that Munc13-4 might function to promote the fusion of $Rab11^+$ with $Rab7^+$ membranes (Menager *et al.*, 2007). However, our studies were unable to determine whether a $Rab11^+$ endosome merge with $Rab7^+$ vacuoles required Munc13-4 because earlier fusion steps in the vacuole assembly pathway failed to occur in Munc13-4–knockdown cells. Unlike cytotoxic T-cells (Menager *et al.*, 2007) or neutrophils (Johnson *et al.*, 2016), we did not detect Munc13-4 on $Rab11^+$ endosomes. The important execution point for Ca^{2+}-activated Munc13-4 in the RBL-2H3 cells was at homotypic SG fusion, which initiates vacuole formation. This reveals that Munc13-4 functions in the Ca^{2+}-triggered fusion of endosomal SGs in mast cells, where it serves as a Ca^{2+} sensor. The role for Munc13-4 in Ca^{2+}-triggered endosome fusion characterized here is different from that in studies in cytotoxic T-cells (Menager *et al.*, 2007) or neutrophils (He *et al.*, 2016), in which Munc13-4–dependent endosome fusion was observed in resting rather than Ca^{2+}-stimulated cells, but local Ca^{2+} increases might activate Munc13-4 in these cases.

Munc13-4 associates with LE SNARE protein complexes

The R-SNARE VAMP8 is a common denominator for Munc13-4–dependent fusion events in RBL-2H3 cells because VAMP8 resides on SGs. For SG exocytosis, VAMP8 pairs with syntaxin-4 and SNAP-23 (Paumet *et al.*, 2000; Lorentz *et al.*, 2012; Wesolowski and Paumet, 2014), and we found that Ca^{2+}-activated Munc13-4 accelerates fusion between VAMP8- and syntaxin1/SNAP25-containing liposomes, similar to results of a recent study using syntaxin2/SNAP23 acceptor liposomes (Chicka *et al.*, 2016). By contrast, homotypic LE fusion uses VAMP8 paired with syntaxin-7, syntaxin-8, and Vti1b (Antonin *et al.*, 2000, 2002). Munc13-4 promoted Ca^{2+}-stimulated liposome fusion using these LE R- and Q-SNARE proteins. We also

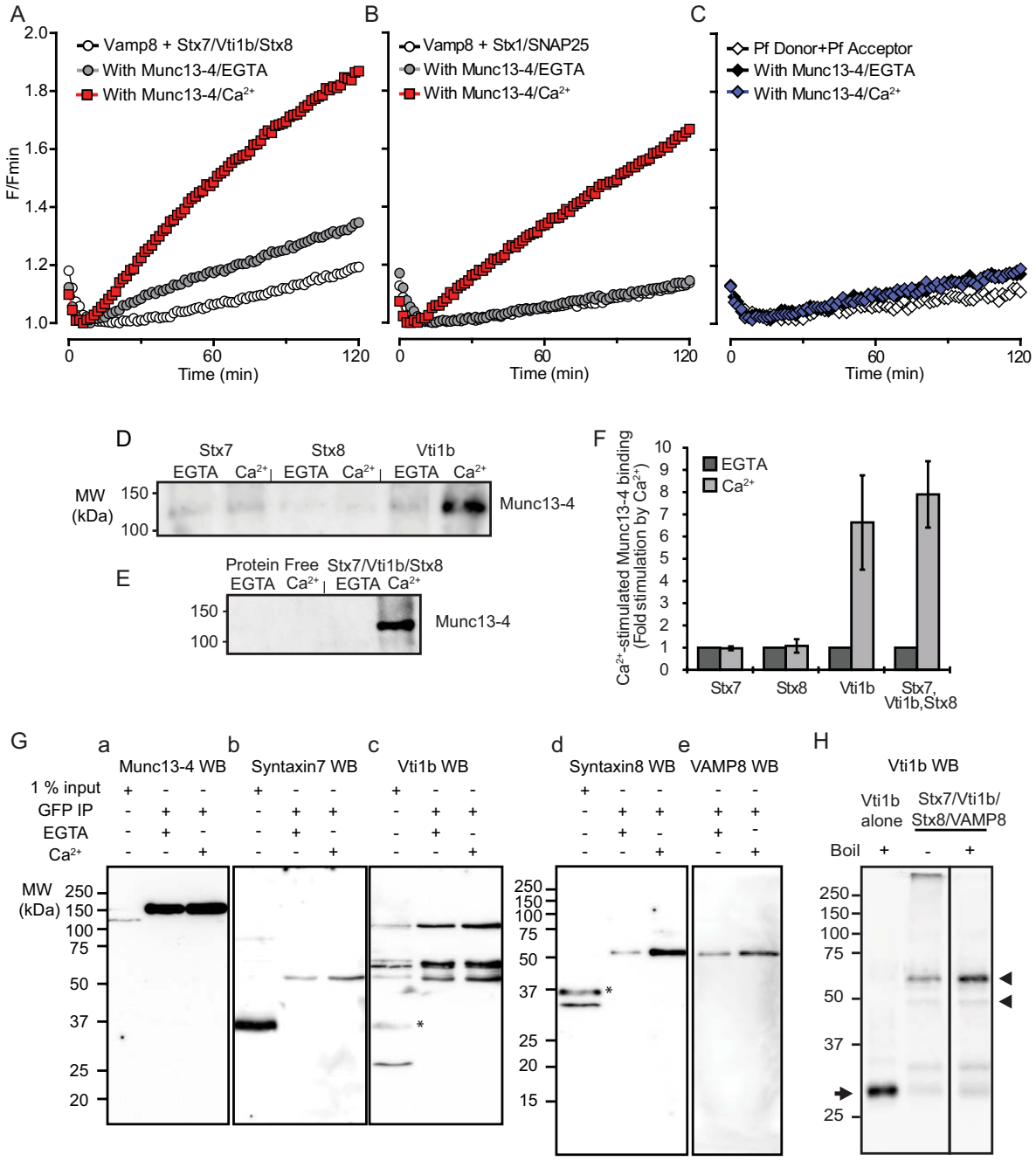

FIGURE 6: Ca^{2+}-activated Munc13-4–dependent liposome fusion. (A) Liposome fusion was detected by dil-diD FRET between VAMP8- and syntaxin7/Vti1b/syntaxin8-containing liposomes without additions (open circles), with 1 μM Munc13-4 (gray circles), or with Munc13-4 plus 300 μM Ca^{2+} (red circles). (B) Fusion of liposomes containing VAMP8 and syntaxin1/SNAP25 was detected in the absence of additions (open circles), with 1 μM Munc13-4 (gray circles), or with Munc13-4 and 300 μM Ca^{2+} (red squares). (C) Protein-free (Pf) liposomes exhibited little fusion in the incubations conditions tested with no additions (open diamond), with 1 μM Munc13-4 (black diamonds), or with Munc13-4 and 300 μM Ca^{2+} (blue diamonds). (D, E) Munc13-4 binding to liposomes reconstituted with the indicated LE Q-SNAREs or protein free was detected in liposome flotation studies either with EGTA or Ca^{2+}. Binding studies were conducted under the same conditions as in A with 1 μM Munc13-4 and EGTA or 300 μM Ca^{2+} as indicated. (F) Western blots as in D and E were quantitated and are presented as fold stimulation comparing signals with Ca^{2+} to those with EGTA (means ± SD, $N = 3$). Proteins used in these studies are shown in Supplemental Figure S4. (G) EGFP-Munc13-4 expressed in RBL-2H3 cells was immunoprecipitated with GFP-Trap nanobody from detergent lysates that included EGTA or $CaCl_2$ (100 μM). Immunoprecipitates were eluted by boiling in SDS sample buffer, run on SDS–PAGE, and immunoblotted for (a) Munc13-4, (b) syntaxin-7, (c) Vti1b, (d) syntaxin-8, and (e) VAMP8 as indicated. Blots were probed sequentially with several antibodies to determine whether bands were immunoreactive for different LE SNAREs or were probed individually with multiple distinct antibodies; two different antibodies detected VAMP8 in e; the results shown are representative of three independent studies for each SNARE. LE SNARE antibodies specifically recognized monomeric LE SNAREs in input lanes (syntaxin-7, 33.5 kDa; Vti1b, 26.1 kDa; syntaxin-8, 30.7 kDa; VAMP8, 13.6 kDa [not shown]). Band assignments for

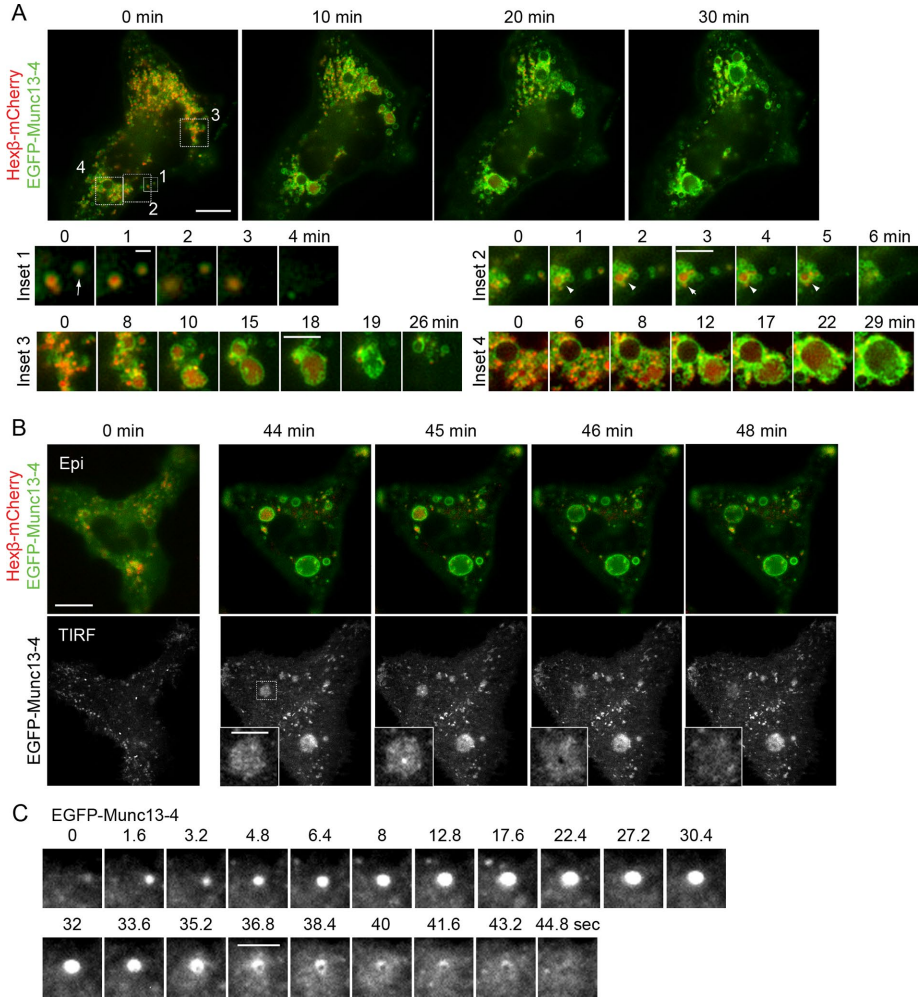

FIGURE 7: Exocytosis of Ca^{2+}-induced vacuoles. (A) Vacuole formation and exocytosis were observed in response to ionomycin stimulation in live-cell studies with EGFP-Munc13-4– and Hexβ-mCherry–expressing cells by epifluorescence. Insets, several distinct modes of exocytosis for SGs and vacuoles from areas boxed in the main image: 1) SG (arrow) and small vacuole lose β-hexosaminidase content; 2) small vacuole (arrowhead) grows before loss of content; 3) larger vacuole grows before loss of content; 4) many SGs contribute to formation of a vacuole that then merges with a vacuole that had already lost content. Incubation times after ionomycin treatment are indicated. (B) Exocytosis of Ca^{2+}-induced vacuoles in EGFP-Munc13-4– and Hexβ-mCherry–expressing cells detected by epifluorescence (top) and TIRF microscopy (bottom). Times after ionomycin treatment are indicated. The smaller of the two vacuoles had formed at 5 min, whereas the larger formed at 10 min after stimulation. The larger vacuole underwent exocytosis at 20 min, losing Hexβ-mCherry but preserving vacuole morphology, indicating a cavicapture mode. The smaller vacuole (boxed) underwent exocytosis in the 44- to 48-min interval, shown losing Hexβ-mCherry by 46 min (top) and diffusing EGFP-Munc13-4 onto the plasma membrane (insets) after fusion pore formation at 46 min (bottom). Scale bars,10 μm (whole cells) 1 μm (A, inset 1), 3 μm (other insets). (C) SG exocytosis in EGFP-Munc13-4–expressing cell imaged by TIRF microscopy. The 0-s frame was from an image acquired 132.8 s after ionomycin treatment. Selected frames from 1.6-s interval recording are shown, indicating diffusion of EGFP-Munc13-4 into plasma membrane. Scale bar, 3 μm.

found that Munc13-4 directly associates with LE SNARE protein complexes in a Ca^{2+}-stimulated manner. In liposome flotation studies with purified proteins, Munc13-4 exhibited Ca^{2+}-dependent binding to liposomes reconstituted with Vti1b or syntaxin-7/Vti1b/syntaxin-8 complexes but not with protein-free liposomes. However, immunoprecipitates of GFP-Munc13-4 in RBL-2H3 cells indicated that Munc13-4 associates with LE SNARE protein complexes, including Vti1b homodimers and homotetramers rather than with SNARE protein monomers. Vti1b exhibits strong self-associations as a transmembrane protein (Mascia and Langosch, 2007), and it is likely that the preferential binding of Munc13-4 to Vti1b- and Q-SNARE-containing liposomes reflected this preference for binding to LE SNARE protein complexes. The additional LE SNARE protein complexes that coprecipitated with Munc13-4 were highly stable, ~50-kDa heterodimeric complexes detected with multiple antibodies, which consisted of syntaxin-7/VAMP8 and Vti1b/syntaxin-8, as well as oligomeric Vti1b. These were likely generated from Munc13-4 bound from multimeric heterotetrameric LE SNARE complexes subjected to boiling and SDS–PAGE (Mascia and Langosch, 2007).

A Ca^{2+}-dependent association of Munc13-4 with syntaxin-7 but not Vti1b or syntaxin-8 in HEK cell lysates was recently reported (He *et al.*, 2016). However, these studies used cooverexpression of Munc13-4 and individual LE SNARE proteins. By contrast, our studies used a GFP-Munc13-4 protein that localizes normally to membranes in RBL-2H3 cells, and the immunoprecipitates isolated endogenous LE SNARE protein complexes assigned by molecular mass and multiple antibody recognition. The results indicate that endosome docking, priming, or fusion may be driven by the Ca^{2+}-dependent binding of Munc13-4 to endosomal Q-SNAREs with the recruitment of VAMP8 for assembly of SNARE complexes. The liposome fusion and SNARE-binding studies presented here are important in revealing the potential for Munc13-4 to act as a Ca^{2+} sensor in membrane fusion events involving LE SNAREs.

immunoprecipitated complexes based on calculated mass and immunoreactivity were (b) syntaxin-7/VAMP8, (c) Vti1b/syntaxin-8, Vti1b dimer, and Vti1b tetramer (from low to high MW), (d) Vti1b/syntaxin-8, and (e) syntaxin-7/VAMP8. Asterisks in c and d indicate carryover of syntaxin-7 immunoreactivity in reprobed blots. There was essentially no cross-reaction between LE SNARE antibodies under these conditions. (H) Endosomal SNARE complexes collapse to 50- to 58-kDa SNARE complexes with boiling. Purified liposomal Vti1b (first lane) or Vti1b, syntaxin-7, Vti1b, and syntaxin-8 (at 1:1:1:1 M ratios) were incubated for 2 h at 37°C and separated by SDS–PAGE without (second lane) or with boiling (third lane); Vti1b was detected by Western blotting as monomer (arrow) or as complexes containing Vti1b (arrowheads). High-MW SNARE complexes near the top of the gel (lane 2) collapse partially in SDS–PAGE and fully with boiling (lane 3). Proteins used in these studies are shown in Supplemental Figure S4.

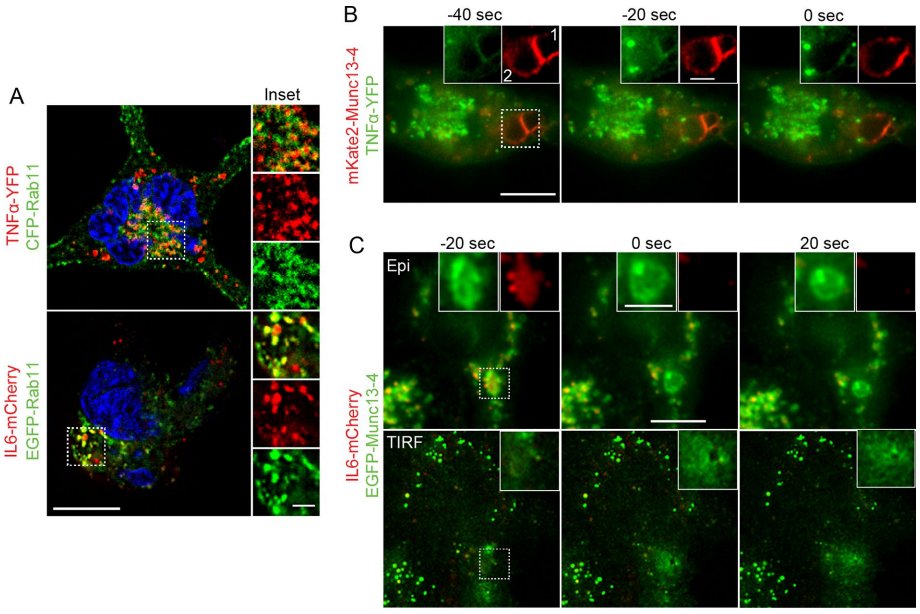

FIGURE 8: Different cargoes released by vacuoles. (A) Trafficking of cytokines in Rab11$^+$ endosomes. Single *z*-slices of confocal images for cells expressing CFP-Rab11 with TNFα-YFP (top) or EGFP-Rab11 with IL-6 mCherry (bottom). The Pearson *r* (cell wide) for these colocalizations was 0.35 ± 0.08 (±SD, $n = 4$) and 0.46 ± 0.15 (±SD, $n = 4$), respectively. Cells were fixed at 6 h posttransfection. (B) TNFα-YFP release from vacuoles in ionomycin-stimulated cells. TNFα-YFP–containing vesicles appear on an mKate2-Munc13-4$^+$ vacuole at −20 s, and the vacuole acquires a luminal green signal that quickly disappears in the next frame (0 s), indicating an exocytic event. Vacuole exocytosis may have occurred by a merge with an adjoining vacuole (see Supplemental Video S7). Images were acquired by epifluorescence at 6 h posttransfection. (C) Simultaneous epifluorescence-TIRF imaging indicated that vacuole-plasma membrane fusion allows IL-6 release. An EFGP-Munc13-4$^+$ vacuole in an ionomycin-stimulated cell containing luminal IL-6-mCherry and associated IL-6 vesicle (–20 s) quickly released contents upon fusion pore opening (0 s). Images were acquired at 2 d posttransfection. Scale bars, 10 μm (whole cells), 3 μm (insets).

In RBL-2H3 cells, Munc13-4 was associated with membranes that underwent fusion. A key element for the specificity of Munc13-4 in membrane fusion events may be its association with at least one of the fusion partner membranes. The membrane association of Munc13-4 may be mediated by Rab27b, with which it strongly colocalizes on SGs or vacuoles. However, Munc13-4 lacking a Rab27 interaction domain was reported to localize to SGs in RBL-2H3 cells (Elstak *et al.*, 2011). This may be explained by the finding that Munc13-4 interacts with multiple Rab proteins such as Rab15, Rab11, Rab27a, Rab37, and Rab22a (Masuda *et al.*, 2000; Shirakawa *et al.*, 2004; Neeft *et al.*, 2005; Zografou *et al.*, 2012; Singh *et al.*, 2013; Higashio *et al.*, 2016; Johnson *et al.*, 2016). Rab27 is nonetheless required for Munc13-4 function in SG exocytosis in RBL-2H3 cells (Neeft *et al.*, 2005; Elstak *et al.*, 2011; Singh *et al.*, 2013). Studies have also documented Ca^{2+}-dependent interactions of soluble Munc13-4 with membranes mediated by its C-terminal C2B domain (Boswell *et al.*, 2012; Chicka *et al.*, 2016). Rab-bound Munc13-4 on a donor membrane could bridge to an acceptor membrane in a Ca^{2+}-stimulated cell and mediate SG docking to the plasma membrane for heterotypic fusion or to other SGs for homotypic fusion (Elstak *et al.*, 2011; Johnson *et al.*, 2011; Chicka *et al.*, 2016). Thus the membrane association of Munc13-4 by a particular set of Rab GTPases may determine specificity of Munc13-4–promoted membrane fusion (Higashio *et al.*, 2016).

Function of exocytic vacuole and compound exocytosis

Classically, stimulated mast cells, as well as other hematopoietic secretory cells, exocytose mediators by both simple and compound exocytosis. In RBL-2H3 cells, stimulated β-hexosaminidase secretion occurs from SGs, as well as from variable-size endosomal vacuoles (Figure 9). One mode of compound exocytosis is multigranular, in which SGs merge homotypically to form larger exocytic structures, which have been characterized in mast cells and basophils by electron microscopy (Lawson *et al.*, 1977; Chandler and Heuser, 1980; Dvorak *et al.*, 1981; Dvorak, 2005). However, the mechanisms responsible for multigranular compound exocytosis have not been previously elucidated. The present work indicates that Ca^{2+}-triggered multigranular compound exocytosis is mediated by Ca^{2+}-activated Munc13-4 acting to promote exocytic vacuole assembly through the homotypic fusion of SGs. That homotypic endosomal fusion may be mediated by a Rab/Munc13-4 complex could account for the finding that both Ca^{2+} and stable GTP analogues promote multigranular compound exocytosis in mast cells and eosinophils (Alvarez de Toledo and Fernandez, 1990; Hartmann *et al.*, 2003). Multigranular compound exocytosis also occurs in many other cells triggered by high Ca^{2+}, such as pancreatic β-cells, endothelial cells, neutrophils, and neurons (Lollike *et al.*, 2002; He *et al.*, 2009; Valentijn *et al.*, 2010; Hoppa *et al.*, 2012). It will be important to assess Munc13-4's role in these cell types.

Compound exocytic vacuoles were surprisingly complex in RBL-2H3 cells containing SG membranes and cargo as well as LE and RE membranes. Mast cells contain SGs of several types, including granules that are multivesicular endosomes (Raposo *et al.*, 1997; Grimberg *et al.*, 2003). As these merge to assemble an enlarged vacuole, the vacuole retains its multivesicular body characteristics (Savina *et al.*, 2005).

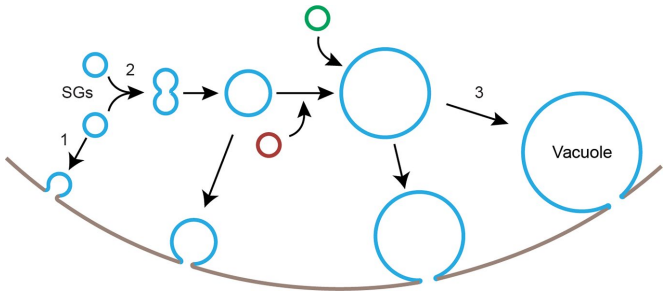

FIGURE 9: Summary of Munc13-4–dependent SG exocytosis and vacuole generation in ionomycin-treated RBL-2H3 cells. Membranes (SGs, vacuoles) containing Munc13-4 are indicated in blue. Rab11$^+$ endosomes and LAMP2$^+$ endosomes are indicated in green and red, respectively. LAMP2$^+$ endosomes merge with vacuoles earlier than Rab11$^+$ endosomes (not shown). Ca^{2+} increases promoted SG exocytosis (1) as well as homotypic SG fusion (2) to form vacuoles that grow by LE and RE addition. SGs and vacuoles of various sizes undergo exocytosis in stimulated cells (3). The present study indicates that Ca^{2+}-bound Munc13-4 operates at 1 and 2, but additional sites of action, such as at the merge of Rab11 REs with vacuoles or at vacuole exocytosis, are possible but not yet experimentally shown.

Note that vacuolar surface markers used throughout these studies (Munc13-4, Rab7, Rab27b, VAMP7, VAMP8) were detected to various extents as puncta within vacuoles, consistent with their reported presence on exosomes as documented in ExoCarta (Keerthikumar *et al.*, 2016). Invagination of the multivesicular body membrane to generate ILVs may operate basally to internalize these membrane-associated proteins.

Vacuoles in Ca^{2+}-stimulated RBL-2H3 cells acquired Rab11 after homotypic SG fusion events generated Munc13-4$^+$/Rab7$^+$ prevacuolar intermediates (Figure 4). The merge of Rab11$^+$ endosomes with the vacuole may convey Rab11 to vacuoles for vacuole exocytosis. Rab11 is involved in the exocytic fusion of REs and multivesicular bodies with the plasma membrane (Savina *et al.*, 2005; Takahashi *et al.*, 2012) and could activate Munc13-4 on the vacuole for vacuole exocytosis (Johnson *et al.*, 2016). In addition, Rab11$^+$ REs deliver additional cargo from the Golgi to the vacuole. Cytokines are trafficked from the Golgi by Rab11$^+$ REs in macrophages (Manderson *et al.*, 2007; Lacy and Stow, 2011; Stow and Murray, 2013). Although cytokine secretion from mast cells may occur largely by pathways distinct from mediator release (Blank *et al.*, 2014), cytokines may also be delivered to multigranular vacuoles for cosecretion. We tested this concept by expressing fluorescent versions of TNFα and IL-6. At early times after transfection, a significant fraction of the newly synthesized cytokines colocalized with Rab11 transport vesicles (Figure 8A). Ionomycin stimulation of the cells resulted in TNFα delivery into the vacuole and subsequent release upon vacuole exocytosis (Figure 8B), which suggests that direct delivery of TNFα from the Golgi to vacuoles is mediated by Rab11$^+$ REs. IL-6 also colocalized with Rab11$^+$ endosomes at early times after transfection (Figure 8A), but the delivery of IL-6 to the vacuole and its subsequent release by vacuole exocytosis in Ca^{2+}-stimulated cells was only detected at late times after transfection (Figure 8D), which suggests a more extended trafficking itinerary from the Golgi to vacuole for IL-6. These studies support the conclusion that vacuoles are highly heterogeneous for cargo derived from multiple trafficking pathways. Thus these organelles assembled for multigranular compound exocytosis represent a collection point for the delayed secretion of multiple constituents. Exocytic vacuoles may be polarized in mast cells for efficiently responding to localized pathogens or immune complexes, as suggested by recent studies (Carroll-Portillo *et al.*, 2010; Joulia *et al.*, 2015).

The Ca^{2+} increases and membrane-associated Munc13-4 lead to the de novo generation of a new exocytic organelle in mast cells. Our findings provide the first molecular description of the formation of multigranular compound exocytic structures. There are apparent parallels between exocytic vacuole formation in mast cells and the generation of cytotoxic granules in T-cells, in which both are hybrid endosomal exocytic organelles. There are nonetheless differences in how the endosomal fusion machinery is used in mast cells and cytotoxic T-cells. Munc13-4 localizes to Rab11 endosomes in cytotoxic T-cells and possibly catalyzes the merge of Rab11 endosomes with Rab7$^+$/Rab27b$^+$ endosomes to generate a precursor to cytotoxic granules (Menager *et al.*, 2007; van der Sluijs *et al.*, 2013). By contrast, Munc13-4 localizes to the Rab7$^+$/Rab27b$^+$ vacuole during a merge with Rab11$^+$ endosomes in mast cells. Future studies will need to clarify the basis for the membrane localization of Munc13-4, which is critical for localizing its function.

MATERIALS AND METHODS

Cells and materials

RBL-2H3 cells (CRL-2256; American Type Culture Collection, Manassas, VA) were cultured in MEM supplemented with 15% fetal bovine serum (FBS) and Antibiotic-Antimycotic (Life Technologies, Carlsbad, CA). 293FT cells (Life Technologies) used for lentivirus production were cultured in DMEM supplemented with 10% FBS, Antibiotic-Antimycotic, and 500 µg/ml Geneticin (Life Technologies). Cells were maintained at 37°C in a 5% CO_2 atmosphere. Lentiviral shRNA constructs for rat Munc13-4 designed by the TRC Consortium were purchased from Sigma-Aldrich (TRCN0000381377; St. Louis, MO) and Open Biosystems (TRCN0000027704; Lafayette, CO). pLKO.1 plasmid was purchased from Sigma-Aldrich. pMD2g and pCMV ΔR8.74 constructs for lentivirus production were purchased from Addgene. pLVX-mCherry plasmid was purchased from Clontech (Mountain View, CA). To generate lenti-hMunc13-4 or mutant hMunc13-4 (Boswell *et al.*, 2012), open reading frames (ORFs) were subcloned into the pLVX plasmid after removal of the mCherry ORF. The mCherry-Rab7 construct was a kind gift from A. Sorkin (University of Pittsburgh, Pittsburgh, PA), and pEGFP-Rab7 was purchased from Addgene. pmKate2-Munc13-4 and pEGFP-Munc13-4 were generated by inserting human Munc13-4 cDNA into pmKate2-C1 (Evrogen, Moscow, Russia) or pEGFP-C1 (Clontech) plasmids. Plasmids for mouse Hexβ-mCherry plasmid and mouse IL-6–mCherry were purchased from Genecopoeia (Rockville, MD). TNFα-YFP construct was a kind gift from M. Olszewski (International Institute of Molecular and Cell Biology, Warsaw, Poland), and the CFP-Rab11 construct was a kind gift from M. Zerial (Max Planck Institute for Molecular Cell Biology and Genetics, Dresden, Germany). LAMP2-mCherry construct was a kind gift from A. Lakkaraju (University of Wisconsin–Madison, Madison, WI). Antibodies used were goat polyclonal Munc13-4 antibody (residue 967–980 amino acids; NB100-41385; used at 5–10 µg/ml for immunofluorescence) from Novus Biologicals (Littleton, CO) and rabbit polyclonal Munc13-4 antibody (full length; H00201294-D01P; used at 5–10 µg/ml for immunofluorescence) from Abnova (Taipei City, Taiwan). These are characterized for immunofluorescence in Supplemental Figure S2. Rabbit polyclonal Munc13-4 C2A antibody was generously provided by H. Horiuchi (Tohoku University, Sendai, Japan); rabbit polyclonal VMAT-2 antibody, used at 1:1000, was generously provided by A. Ruoho (University of Wisconsin–Madison); rabbit polyclonal Rab27b antibody was purchased from Synaptic Systems (Goettingen, Germany; 168103; used at 5–10 µg/ml for immunofluorescence); sheep polyclonal syntaxin-7 antibody (AF5478; 1µg/ml for Western blotting), goat polyclonal VAMP8 antibody (AF5354; 1 µg/ml for Western blotting), and sheep polyclonal syntaxin-8 antibody (AF5448; 1 µg/ml for Western blotting) were purchased from R&D systems (Minneapolis, MN); another rabbit polyclonal antibody against VAMP8 was generously provided by G. Groblewski (University of Wisconsin–Madison; 1:3000 dilution for Western blotting); rabbit polyclonal Vti1b antibody was purchased from Sigma-Aldrich (SAB1410097; 1 µg/ml for Western blotting); and Alexa fluorophore–conjugated secondary antibodies were from Molecular Probes (Eugene, OR). Monoclonal anti–2,4-dinitrophenol (DNP) IgE, DNP–human serum albumin (HSA), ionomycin, thapsigargin, and the β-hexosaminidase substrate *p*-nitrophenyl *N*-acetyl-β-D-glucosaminide (pNAG) were from Sigma-Aldrich.

Lentivirus transduction and generation of stable clones

Lentiviruses were produced as in Berger *et al.* (2011) with modifications. 293FT cells were transfected with 6 µg of pMD2.G, 15 µg of pCMV ΔR8.74, and 20 µg of shRNA plasmid per 10-cm dish by $CaPO_4$ precipitation. At 24 h after transfection, media were replaced by complete growth medium added with 11 µg/ml BSA. Supernatants were collected at 48 and 72 h after transfection. Supernatants were concentrated 200-fold by 2 h of sedimentation at 110,000 × *g*

and resuspended in phosphate-buffered saline (PBS) by swirling overnight. The virus solution was aliquoted for frozen storage at −80°C. Genomic RNA from the lentivirus was purified, and copy numbers of lentivirus for an aliquot were determined using Lenti-X qRT-PCR Titration Kit (Clontech) following the manufacturer's protocol. Lentivirus infection was achieved by incubating cells with lentivirus and 10 μg/ml protamine sulfate. Munc13-4–deficient clones were selected in the presence of 0.7 μg/ml puromycin for 10–14 d with periodic medium replacement. We generated 35 stable clones, the majority of which exhibited reduced or absent Munc13-4 protein expression that correlated with reduced secretion. Results reported are representative from several stable clones. In rescue studies, a lentivirus carrying pLKO.1 vector served as a sham control. To express hMunc13-4 in knockdown (KD) cells, 48 h of infection was typically sufficient to achieve normal cell levels of expression. Ongoing suppression of endogenous Munc13-4 in rescue studies was verified by quantitative reverse transcription PCR (qRT-PCR) for the rat Munc13-4 transcript. A lentivirus that carries pLVX-mCherry served as a sham control unless there was a conflict for multichannel fluorescence microscopy. To compare C2 domain mutants with WT Munc13-4, we infected 2×10^4 copy of each lentivirus in 7.5×10^3 KD cells. To monitor variation in rescue, multiple clones were infected with hMunc13-4 lentivirus, which showed a comparable frequency of vacuole formation upon ionomycin stimulation.

qRT-PCR

Total RNAs were extracted from cells by TRIzol reagent (Life Technologies) according to the manufacturer's protocol. DNA carryovers were digested by incubation of the total RNAs with DNase I (New England Biolabs, Ipswich, MA) for 30 min at 37°C, and the enzyme was inactivated by incubation at 75°C for 10 min. RNA concentration was determined by NanoDrop (Thermo Scientific, Waltham, MA). A 1-μg amount of total RNA was subject to a reverse transcription using Affinity Script reverse transcriptase (Agilent Technologies, Santa Clara, CA) with oligo d(T) primer according to the manufacturer's protocol. Endogenous rMunc13-4 cDNA was amplified by Brilliant II SYBR Green PCR Master Mix (Agilent Technologies) using forward primer ATCGATGCCAAGGGGTCGA and reverse primer GTCAGTCCAGGTACCCTGCAG, and the amount of amplification was monitored by ABI7500 Fast System (Life Technologies). As a reference gene, rat β-actin cDNA was amplified and detected by the same method using forward primer AGGCCAACCGTGAAAAGATG and reverse primer GGTACGACCAGAGGCATACA. Cycle threshold was determined for rMunc13-4 and β-actin from the amplification curves acquired by 7500 Software (Life Technologies). Relative expression was calculated by the $E\Delta\Delta^{Ct}$ method using *Ct* values of parental RBL cell samples as controls (Pfaffl, 2001).

Secretion assays

β-Hexosaminidase was determined by its enzymatic activity for chromogenic substrate pNAG. Cells were seeded in 96-well microwell culture plates and stimulated in Tyrode's buffer (130 mM NaCl, 5 mM KCl, 1 mM $MgCl_2$, 20 mM 4-(2-hydroxyethyl)-1-piperazineethanesulfonic acid (HEPES), 5.6 mM glucose, 0.5 mg/ml bovine serum albumin [BSA], pH 7.4) with various concentration of $CaCl_2$ in the presence or absence of 2.5 μM ionomycin at 37°C for 20 min. Supernatants were transferred to microtiter assay plates, and the remaining cells were lysed by 1% Triton X-100 for 5 min at room temperature. Portions of supernatants and lysates were subject to incubation with 8 mM pNAG in buffer (0.1 M citrate, 0.2 M Na_2HPO_4, pH 4.5). Subsequent enzyme reactions were conducted for 1 h at 37°C. The reaction was stopped and developed by addition of glycine stop buffer (0.2 M glycine, 0.2 M NaCl, 0.2 M NaOH, pH 10). Conversion of pNAG to yellow was read at 405 nm, with background subtraction of absorbance at 630 nm. The absorbance values of supernatant and lysate were combined for total β-hexosaminidase activity, and secretion was plotted by calculating the enzyme activity in supernatant as percentage of total activity. The Ca^{2+} dose–response curves were analyzed by nonlinear least squares fits with the model equation % secretion = % secretion$_{min}$ + (% secretion$_{max}$ − % secretion$_{min}$)/(1 + $10^{(\log EC50 \_ \log[Ca2+]) \times slope}$) using R software. Variable slopes do not improve curve fits and therefore did not bring any significant difference to curve fitting. Consequently a slope value 1.3, which was determined for wild-type rescue samples, was applied for all the curves, with other parameters variable. Best-fitting models were visualized by Prism software (GraphPad) and the model fitting analysis was conducted through consultation with the University of Wisconsin Institute for Clinical and Translational Research (Mary Lindstrom, University of Wisconsin–Madison).

Immunoblotting

RBL cells were washed and solubilized by ice-cold 1% Triton X-100 in PBS in the presence of a protease inhibitor cocktail and 1 mM phenylmethanesulfonyl fluoride for 10 min at 4°C with gentle rocking. The lysate was cleared by centrifugation at 16,000 × *g* for 5 min at 4°C. SDS was added to 2% final concentration, and lysate was boiled for 5 min at 96°C. The boiled lysates were cleared by centrifugation, and protein concentration was determined by BCA Assay Kit (Pierce Chemical, Rockford, IL). Between 20 and 30 μg of lysate protein was mixed with 4× SDS sample buffer (250 mM Tris-HCl, pH 6.8, 30% glycerol, 300 mM dithiothreitol [DTT], 8% SDS, 0.02% bromophenol blue) and boiled for 5 min at 96°C before loading on 8% polyacrylamide gels. After electrophoresis (Bio-Rad, Hercules, CA), the proteins in the gel were electrotransferred to nitrocellulose membranes (0.45-μm pore; Bio-Rad). Membranes were blocked with 5% skim milk in PBST (PBS with 0.1% Triton X-100) for 1 h at room temperature and incubated with Munc13-4 antibodies diluted in 1:5000 ratio (rabbit polyclonal antibody against residues 1–262 of hMunc13-4 [Boswell *et al.*, 2012] or goat polyclonal antibody against residues 967–980 of hMunc13-4 [Abnova]) in 5% BSA in PBST overnight. Primary antibody was detected by incubation with horseradish peroxidase–conjugated secondary antibodies for 2 h at room temperature. Blots were developed by an enhanced chemiluminescence kit (Pierce) and imaged by an ImageQuant LAS 4000 system (GE Healthcare, Pittsburgh, PA). Band intensity was quantified by image analysis using ImageJ software.

Transfection and immunofluorescence

For fluorescence microscopy, glass coverslips were coated with 0.1 mg/ml poly-D-lysine and 30 μg/ml bovine fibronectin at 37°C (Sigma-Aldrich). To express fluorescence-tagged proteins, 2 μg of DNA was mixed with RBL cells suspended in Cytomix buffer including 5 mM glutathione and 2 mM ATP in a 1-mm-gap electroporation cuvette (van den Hoff *et al.*, 1992). The mixture was electroshocked by two consecutive 225-V pulses with 1-ms duration using an ECM830 electroporator (Harvard Apparatus, Holliston, MA). Media were replaced after 24 h, and the constructs typically expressed fluorescence proteins after 48 h of incubation. For stimulation, cells were incubated in Tyrode's buffer with 10 mM $CaCl_2$ in the presence or absence of 2.5 μM ionomycin generally for 20 min. For antigen stimulation, cells were primed with 200 ng/ml anti-DNP monoclonal IgE in growth medium overnight and subsequently washed with Tyrode's buffer and incubated with 50 ng/ml DNP-HSA in Tyrode's buffer containing

10 mM $CaCl_2$ for 20 min. Alternatively, RBL cells were stimulated with 1 µM thapsigargin in 10 mM Ca^{2+}–containing Tyrode's buffer. For live-cell imaging, glass-bottom culture dishes (MatTek, Ashland, MA) were coated with poly-D-lysine (0.1 mg/ml) at 37°C for 30 min, followed by coating with fibronectin (33 µg/ml) at 37°C for 30 min. For immunostaining, cells were washed and fixed in 4% formaldehyde in PBS for 30 min at room temperature and permeabilized with 0.2% Triton X-100 in PBS for 20 min at room temperature. Nonspecific binding was blocked by incubating with 5% FBS or goat or donkey serum for 1 h. The cells were incubated with primary antibodies diluted in the blocking solution overnight at 4°C. The cells were washed and incubated with 20 µg/ml Alexa Fluor–conjugated secondary antibodies for 1 h at room temperature. After additional washing, nuclei were stained with 2 µg/ml Hoechst 33342 for 5 min at room temperature. Cells attached to glass coverslip were buffered by Slowfade Gold solution (Life technologies) and mounted on glass slides.

Fluorescence microscopy and image analysis

Cells were imaged by epifluorescence or TIRF illumination using a Nikon Eclipse Ti microscope controlled by NIS element software. Images were captured with an iXon Ultra EM-CCD camera through a Nikon APO 100× TIRF numerical aperture (NA) 1.49 objective. Time-lapse imaging for live cells was conducted in a humidified imaging chamber maintained at 37°C (Tokai Hit, Shizuoka-ken, Japan). Simultaneous epi-TIRF images were acquired using different Perfect Focus System offset values for epifluorescence and TIRF channels. The switching time between epifluorescence and TIRF channels was <1 s. The SIM images were acquired with a Nikon N SIM microscope (SR-APO TIRF NA 1.49 100× lens, Andor iXon 3 EM-CCD camera, and 408-, 488-, 561-, and 640-nm laser lines) using three-dimensional (3D) SIM mode and reconstructed with NIS software. Confocal images were acquired with a Nikon $A1R^+$ confocal system using GaAsP detectors. Epifluorescence and confocal images were deconvolved, processed, and analyzed by NIS software (Nikon, Tokyo, Japan). Epifluorescence images were deconvolved by two-dimensional (2D) blind or 2D Landweber algorithm with one to five iterations. Confocal images were deconvolved by the 3D Landweber algorithm with five iterations. Deconvolution artifacts were checked by line scan analysis comparing with original images. For fluorescence overlap analysis, Manders' overlap coefficient was calculated by JACoP plug-in in ImageJ for fluorescent pixels above threshold (Bolte and Cordelieres, 2006). Fluorescence channels were typically arranged as red fluorescence, channel 1; and green fluorescence, channel 2, in JACoP plug-in. Manders' coefficients produced by JACoP included M1 and M2, where M1 was fraction of channel 1 overlapping with channel 2, and M2 was fraction of channel 2 overlapping with channel 1. Channel arrangements are indicated in the figure legends. Pearson's *r* for Figure 8B was calculated by NIS software. For vesicle profile area determination, images were binarized by threshold function, and circular objects were detected by particle analysis function in ImageJ software. The diffusion coefficient of EGFP-Munc13-4 was calculated as in Zenisek *et al.* (2002) using ImageJ software. Circular regions of interest (ROIs) were drawn on the image showing fusion pore opening. The first ROI with 2-pixel diameter was located on the position of the fusion pore, and successive ROIs were drawn around the first ROI with a 2-pixel increment in diameter as concentric rings (radial sweeps). The radial sweeps were applied to images before and after fusion pore opening and mean intensities were measured. Mean intensity differences (MIDs) were calculated by subtracting mean intensity values between successive ROIs to calculate Munc13-4 fluorescence spread. The calculated MIDs were fitted into a Gaussian distribution. The Gaussian distribution of fluorescence intensity around the fusion pore and its width parameter σ (SD) were calculated by MATLAB software (MathWorks), and Gaussian distribution curves were generated by Prism software. Squares of σ (in micrometers) values were plotted as a function of time, yielding a linear equation ($\sigma^2 = 0.2784t + 0.3441$; t in seconds), where 0.2784 $\mu m^2/s = 4D$ (D is the diffusion coefficient; Zenisek *et al.*, 2002). For the figures, images were rasterized to 1000 dpi by Photoshop CS3 software (Adobe).

Electron microscopy

RBL cells were maintained adherent on sapphire disks (3 mm in diameter, 0.05 mm in thickness) that were coated with poly-D-lysine and fibronectin. Each substrate was incubated with the disks overnight. The sapphire disks attached with cells were placed on Parafilm M (Bemis, Oshkosh, WI) until cryofixation, which was etched by needles. The disks were dipped in a cryoprotectant 1-hexadecane before being frozen in a high-pressure freezing machine (HPM 010; Balzers). After freezing, cells were dehydrated by freeze substitution in an acetone solution containing 1% osmium and 1% water as described (McDonald *et al.*, 2010). The frozen samples were placed at –85°C for 72 h and then moved to –20°C. Samples were incubated for 24 h at –20°C and brought to– 4°C for 4 h. Finally, the samples were brought up to room temperature for 2 h and rinsed with dry acetone. Rinsed samples were embedded as follows: incubation in resin mixed of 25% Epon and 75% plastic for 1 h, 50% Epon and 50% acetone overnight, 75% Epon and 25% acetone for 1 h, and 100% Epon in vacuum for 4 h, and finally the 100% Epon was polymerized at 60°C for 48 h. The resin-containing cells were sectioned with ~90-nm thickness and contrasted by aqueous 2% uranyl acetate for 5–20 min immediately before imaging under a Philips CM120 STEM system.

GFP-Trap coimmunoprecipitation

RBL cells were transfected with EGFP-Munc13-4 constructs. After 2 d, cells were washed with ice-cold PBS and lysed in a Tris-NaCl buffer (50 mM Tris-Cl, 300 mM NaCl, 0.5% Triton X-100, protease inhibitor cocktail, 1 mM phenylmethanesulfonyl fluoride) for 30 min at 4°C. Cell debris was sedimented by centrifugation at 14,000 rpm for 15 min at 4°C. The supernatant was adjusted to contain 0.3% Triton X-100 and then mixed with GFP-Trap M nanobody (Chromotek, Martinsried, Germany) that had been equilibrated in the lysis buffer containing 0.3% Triton X-100 and washed. $CaCl_2$ (100 µM) or ethylene glycol tetraacetic acid (EGTA; 200 µM) was added in the mixtures, which were incubated for 2 h at 4°C with rotation. After the incubation, the nanobody-lysate mixture was separated on DynaMag-2 (Invitrogen). The immune complexes were washed with the Tris-NaCl buffer containing 0.1% Triton X-100 and then washed with PBS. The immune complexes were boiled in 1× SDS-sample buffer containing 2% SDS and 75 mM DTT for 5 min at 95°C, sedimented at 5000 × *g*, resuspended, and separated on the magnet rack. The solutions containing the dissociated complexes were immediately subjected to SDS–PAGE electrophoresis. Munc13-4 and SNAREs in the elution were detected by Western blotting.

SNARE and Munc13-4 protein purification

Plasmid constructs pTW34 to express rat syntaxin-1A with N-terminally histidine (His)-tagged mouse SNAP-25B were generously provided by J. E. Rothman (Yale University, New Haven, CT) and T. Weber (Mount Sinai School of Medicine, New York, NY), and exocytic neuronal SNARE proteins were purified as described (Weber *et al.*, 1998) by nickel-nitriloacetic acid (Ni NTA; Qiagen, Hilden, Germany) chromatography. Pet28a plasmids expressing

C-terminal His-tagged VAMP-8 and late endosome SNARE proteins syntaxin-7 and -8 and Vti1b were provided by J. Shen (University of Colorado, Boulder, CO) and purified as described (Yu *et al.*, 2013) by Ni-NTA (Qiagen) chromatography. His_6-tagged human Munc13-4 protein produced in insect Sf9 cells was purified on Ni-NTA agarose (Qiagen) and further purified by Mono Q anion exchange chromatography (GE Healthcare) as previously described (Shirakawa *et al.*, 2004).

Proteoliposome preparation

1-Palmitoyl-2-oleoyl phosphocholine (POPC), 1,2-dioleoyl phosphoserine (DOPS), 1,2-dioleoyl phosphoethanolamine (DOPE), and cholesterol were from Avanti Polar Lipids (Alabaster, AL). 1,1′-Dioctadecyl-3,3,3′,3′-tetramethylindocarbocyanine perchlorate (DiI) and 1,1′-dioctadecyl-3,3,3′,3′-tetramethylindodicarbocyanine 4-chlorobenzenesulfonate (DiD) were from Invitrogen-ThermoFisher Scientific. Lipid mixtures were spiked with 2 µl of [^{3}H]1,2-dipalmitoyl PC (~2×10^5 cpm/nmol; Dupont) to determine lipid recoveries and standardize fusion and liposome-binding reactions. Lipid mixtures for reconstituted liposomes mimicked late endosomal lipid composition (Yu *et al.*, 2013). For R-SNARE reconstitution, POPC, DOPE, DOPS, cholesterol, and DiD were mixed at a 58:20:10:10:2% mol ratio. For Q-SNARE reconstitution, POPC, DOPE, DOPS, cholesterol, and DiI were mixed at a 58:20:10:10:2% mol ratio. Lipid mixes were dried under argon gas and resuspended with SNARE proteins in elution buffer (25 mM HEPES-KOH, pH 7.4, 100 mM KCl, 500 mM imidazole-OAc, pH 7.4, and 1.0% β-octylglucoside). SNARE proteoliposomes were made by comicellization with protein:lipid mixes at 1:500 for neuronal or late endosomal/lysosomal Q-SNAREs and 1:200 for R-SNAREs. Detergent was removed by overnight dialysis using Slide-A-Lyzer cassettes (Thermo Scientific) against reconstitution buffer (25 mM HEPES, pH 7.4, 100 mM KCl, 10% [vol/vol] glycerol, and 1 mM DTT) containing SM-2 Biobeads at 1 g/l (Bio-Rad), and all proteoliposomes were purified by Accudenz gradient flotation and further cleaned using 7K Zeba Spin desalting columns (ThermoFisher Scientific).

FRET-based lipid mixing

The lipid-mixing assay between fluorescent donor and acceptor liposomes was performed as previously described (Boswell *et al.*, 2012). The standard assay used 0.45 mM Q-SNARE and 0.225 mM R-SNARE liposomes in a total reaction volume of 75 µl of reconstitution buffer without glycerol supplemented with 0.1 mM EGTA. Munc13-4 protein was added to a final concentration of 1 µM. For the stimulation of Munc13-4 acceleration of SNARE-dependent liposome fusion, calcium was added at a final free concentration of 300 µM. Reactions were assembled on ice and mixed before addition to prewarmed 96-well FluoroNunc plates. Lipid mixing was observed as an increase in fluorescence resonance energy transfer from DiI to DiD labels by measuring DiD (acceptor) fluorescence at 700 ± 5 nm during DiI (donor) excitation at 514 ± 5 nm every 90 s over 2 h at 35°C using the SPECTRAmax GEMINI-XS spectrofluorometer (Molecular Devices, Sunnyvale, CA). Results are expressed as the ratio of fluorescence at time *x*/minimum fluorescence measured over the entire 2 h.

Liposome binding assay

We assessed Munc13-4 binding to protein-free and reconstituted late endosomal Q-SNARE (syntaxin8/syntaxin7/Vti1b)-containing liposomes using buoyant density liposome flotation as previously described (Weber *et al.*, 1998). Binding reactions with protein-free or Q-SNARE liposomes were assembled with 1 µM Munc13-4 in the absence of Ca^{2+} with 0.2 mM EGTA or presence of 300 µM Ca^{2+} (free concentration) and incubated at room temperature for 1 h. Lipid recovery was determined by tracer [^{3}H]PC lipid and matched across all binding reactions. An equal volume of 80% Accudenz was added to binding reactions for a final concentration of 40% Accudenz, transferred to 5 × 41 mm Beckman Ultra-Clear centrifuge tubes, and overlaid with 350 µl of 30% Accudenz and 30 µl of reconstitution buffer. Accudenz gradient solutions contained 0.2 mM EGTA or 300 µM Ca^{2+} as appropriate. Gradients were centrifuged for 4 h at 48,000 rpm in a Beckman SW50.1 rotor with Teflon adaptors. Samples were collected from the 0/30% Accudenz interface and resolved by SDS–PAGE and Western blotting onto nitrocellulose.

Statistical analysis

All statistical significances were examined by unpaired *t* test (*$p < 0.05$, **$p < 0.01$, ***$p < 0.001$).

ACKNOWLEDGMENTS

We acknowledge help provided by Stephen Bruinsma in the early stages of this work. We thank Maciej Olszewski, Marino Zerial, Alexander Sorkin, Arnold Ruoho, and Aparna Lakkaraju for reagents, Ben August for support for electron microscopy imaging, and Mary Lindstrom for support on mathematical model fitting. This work was supported by National Institutes of Health grant DK025861 to T.F.J.M.

REFERENCES

Allersma MW, Wang L, Axelrod D, Holz RW (2004). Visualization of regulated exocytosis with a granule-membrane probe using total internal reflection microscopy. Mol Biol Cell 15, 4658–4668.

Alvarez de Toledo G, Fernandez JM (1990). Patch-clamp measurements reveal multimodal distribution of granule sizes in rat mast cells. J Cell Biol 110, 1033–1039.

Antonin W, Fasshauer D, Becker S, Jahn R, Schneider TR (2002). Crystal structure of the endosomal SNARE complex reveals common structural principles of all SNAREs. Nat Struct Biol 9, 107–111.

Antonin W, Holroyd C, Tikkanen R, Honing S, Jahn R (2000). The R-SNARE endobrevin/VAMP-8 mediates homotypic fusion of early endosomes and late endosomes. Mol Biol Cell 11, 3289–3298.

Azouz NP, Hammel I, Sagi-Eisenberg R (2014a). Characterization of mast cell secretory granules and their cell biology. DNA Cell Biol 33, 647–651.

Azouz NP, Matsui T, Fukuda M, Sagi-Eisenberg R (2012). Decoding the regulation of mast cell exocytosis by networks of Rab GTPases. J Immunol 189, 2169–2180.

Azouz NP, Zur N, Efergan A, Ohbayashi N, Fukuda M, Amihai D, Hammel I, Rothenberg ME, Sagi-Eisenberg R (2014b). Rab5 is a novel regulator of mast cell secretory granules: impact on size, cargo, and exocytosis. J Immunol 192, 4043–4053.

Baker RW, Hughson FM (2016). Chaperoning SNARE assembly and disassembly. Nat Rev Mol Cell Biol 17, 465–479.

Baker RW, Jeffrey PD, Zick M, Phillips BP, Wickner WT, Hughson FM (2015). A direct role for the Sec 1/Munc18-family protein Vps33 as a template for SNARE assembly. Science 349, 1111–1114.

Behrendorff N, Dolai S, Hong W, Gaisano HY, Thorn P (2011). Vesicle-associated membrane protein 8 (VAMP8) is a SNARE (soluble N-ethylmaleimide-sensitive factor attachment protein receptor) selectively required for sequential granule-to-granule fusion. J Biol Chem 286, 29627–29634.

Benado A, Nasagi-Atiya Y, Sagi-Eisenberg R (2009). Protein trafficking in immune cells. Immunobiology 214, 507–525.

Berger G, Durand S, Goujon C, Nguyen XN, Cordeil S, Darlix JL, Cimarelli A (2011). A simple, versatile and efficient method to genetically modify human monocyte-derived dendritic cells with HIV-1-derived lentiviral vectors. Nat Protoc 6, 806–816.

Blank U, Madera-Salcedo IK, Danelli L, Claver J, Tiwari N, Sanchez-Miranda E, Vazquez-Victorio G, Ramirez-Valadez KA, Macias-Silva M, Gonzalez-Espinosa C (2014). Vesicular trafficking and signaling for cytokine and chemokine secretion in mast cells. J Immunol 5, 453.

Bolte S, Cordelieres FP (2006). A guided tour into subcellular colocalization analysis in light microscopy. J Microsc 224, 213–232.
Boswell KL, James DJ, Esquibel JM, Bruinsma S, Shirakawa R, Horiuchi H, Martin TF (2012). Munc13-4 reconstitutes calcium-dependent SNARE-mediated membrane fusion. J Cell Biol 197, 301–312.
Brzezinska AA, Johnson JL, Munafo DB, Crozat K, Beutler B, Kiosses WB, Ellis BA, Catz SD (2008). The Rab27a effectors JFC1/Slp1 and Munc13-4 regulate exocytosis of neutrophil granules. Traffic 9, 2151–2164.
Cao Q, Zhong XZ, Zou Y, Murrell-Lagnado R, Zhu MX, Dong XP (2015). Calcium release through P2X4 activates calmodulin to promote endolysosomal membrane fusion. J Cell Biol 209, 879–894.
Carroll-Portillo A, Spendier K, Pfeiffer J, Griffiths G, Li H, Lidke KA, Oliver JM, Lidke DS, Thomas JL, Wilson BS, Timlin JA (2010). Formation of a mast cell synapse: Fc epsilon RI membrane dynamics upon binding mobile or immobilized ligands on surfaces. J Immunol 184, 1328–1338.
Catz SD (2013). Regulation of vesicular trafficking and leukocyte function by Rab27 GTPases and their effectors. J Leukoc Biol 94, 613–622.
Chandler DE, Heuser JE (1980). Arrest of membrane fusion events in mast cells by quick-freezing. J Cell Biol 86, 666–674.
Chapman ER (2008). How does synaptotagmin trigger neurotransmitter release? Annu Rev Biochem 77, 615–641.
Chicka MC, Ren Q, Richards D, Hellman LM, Zhang J, Fried MG, Whiteheart SW (2016). Role of Munc13-4 as a Ca2+-dependent tether during platelet secretion. Biochem J 473, 627–639.
Cohen R, Corwith K, Holowka D, Baird B (2012). Spatiotemporal resolution of mast cell granule exocytosis reveals correlation with Ca2+ wave initiation. J Cell Sci 125, 2986–2994.
Colombo MI, Beron W, Stahl PD (1997). Calmodulin regulates endosome fusion. J Biol Chem 272, 7707–7712.
Dvorak AM (2005). Ultrastructural studies of human basophils and mast cells. J Histochem Cytochem 53, 1043–1070.
Dvorak AM, Galli SJ, Morgan E, Galli AS, Hammond ME, Dvorak HF (1981). Anaphylactic degranulation of guinea pig basophilic leukocytes. I. Fusion of granule membranes and cytoplasmic vesicles formation and resolution of degranulation sacs. Lab Invest 44, 174–191.
Elstak ED, Neeft M, Nehme NT, Voortman J, Cheung M, Goodarzifard M, Gerritsen HC, van Bergen En Henegouwen PM, Callebaut I, de Saint Basile G, van der Sluijs P (2011). Munc13-4 rab27 complex is specifically required for tethering secretory lysosomes at the plasma membrane. Blood 118, 1570–1578.
Feldmann J, Callebaut I, Raposo G, Certain S, Bacq D, Dumont C, Lambert N, Ouachee-Chardin M, Chedeville G, Tamary H, *et al.* (2003). Munc13-4 is essential for cytolytic granules fusion and is mutated in a form of familial hemophagocytic lymphohistiocytosis (FHL3). Cell 115, 461–473.
Ghislat G, Knecht E (2013). Ca(2)(+)-sensor proteins in the autophagic and endocytic traffic. Curr Protein Peptide Sci 14, 97–110.
Goishi K, Mizuno K, Nakanishi H, Sasaki T (2004). Involvement of Rab27 in antigen-induced histamine release from rat basophilic leukemia 2H3 cells. Biochem Biophys Res Commun 324, 294–301.
Grimberg E, Peng Z, Hammel I, Sagi-Eisenberg R (2003). Synaptotagmin III is a critical factor for the formation of the perinuclear endocytic recycling compartment and determination of secretory granules size. J Cell Sci 116, 145–154.
Groffen AJ, Martens S, Diez Arazola R, Cornelisse LN, Lozovaya N, de Jong AP, Goriounova NA, Habets RL, Takai Y, Borst JG, *et al.* (2010). Doc2b is a high-affinity Ca2+ sensor for spontaneous neurotransmitter release. Science 327, 1614–1618.
Hartmann J, Scepek S, Hafez I, Lindau M (2003). Differential regulation of exocytotic fusion and granule-granule fusion in eosinophils by Ca2+ and GTP analogs. J Biol Chem 278, 44929–44934.
Hay JC (2007). Calcium: a fundamental regulator of intracellular membrane fusion? EMBO Rep 8, 236–240.
He J, Johnson JL, Monfregola J, Ramadass M, Pestonjamasp K, Napolitano G, Zhang J, Catz SD (2016). Munc13-4 interacts with syntaxin 7 and regulates late endosomal maturation, endosomal signaling, and TLR9-initiated cellular responses. Mol Biol Cell 27, 572–587.
He L, Xue L, Xu J, McNeil BD, Bai L, Melicoff E, Adachi R, Wu LG (2009). Compound vesicle fusion increases quantal size and potentiates synaptic transmission. Nature 459, 93–97.
Higashio H, Nishimura N, Ishizaki H, Miyoshi J, Orita S, Sakane A, Sasaki T (2008). Doc2 alpha and Munc13-4 regulate Ca(2+) -dependent secretory lysosome exocytosis in mast cells. J Immunol 180, 4774–4784.
Higashio H, Satoh Y, Saino T (2016). Mast cell degranulation is negatively regulated by the Munc13-4-binding small-guanosine triphosphatase Rab37. Sci Rep 6, 22539.
Holroyd C, Kistner U, Annaert W, Jahn R (1999). Fusion of endosomes involved in synaptic vesicle recycling. Mol Biol Cell 10, 3035–3044.
Hong W, Lev S (2014). Tethering the assembly of SNARE complexes. Trends Cell Biol 24, 35–43.
Hoppa MB, Jones E, Karanauskaite J, Ramracheya R, Braun M, Collins SC, Zhang Q, Clark A, Eliasson L, Genoud C, *et al.* (2012). Multivesicular exocytosis in rat pancreatic beta cells. Diabetologia 55, 1001–1012.
Imig C, Min SW, Krinner S, Arancillo M, Rosenmund C, Sudhof TC, Rhee J, Brose N, Cooper BH (2014). The morphological and molecular nature of synaptic vesicle priming at presynaptic active zones. Neuron 84, 416–431.
Jahn R, Fasshauer D (2012). Molecular machines governing exocytosis of synaptic vesicles. Nature 490, 201–207.
Jahn R, Scheller RH (2006). SNAREs—engines for membrane fusion. Nat Rev Mol Cell Biol 7, 631–643.
James DJ, Martin TF (2013). CAPS and Munc13: CATCHRs that SNARE Vesicles. Front Endocrinol 4, 187.
Johnson JL, He J, Ramadass M, Pestonjamasp K, Kiosses WB, Zhang J, Catz SD (2016). Munc13-4 is a Rab11-binding protein that regulates Rab11-positive vesicle trafficking and docking at the plasma membrane. J Biol Chem 291, 3423–3438.
Johnson JL, Hong H, Monfregola J, Kiosses WB, Catz SD (2011). Munc13-4 restricts motility of Rab27a-expressing vesicles to facilitate lipopolysaccharide-induced priming of exocytosis in neutrophils. J Biol Chem 286, 5647–5656.
Joulia R, Gaudenzio N, Rodrigues M, Lopez J, Blanchard N, Valitutti S, Espinosa E (2015). Mast cells form antibody-dependent degranulatory synapse for dedicated secretion and defence. Nat Commun 6, 6174.
Junge HJ, Rhee JS, Jahn O, Varoqueaux F, Spiess J, Waxham MN, Rosenmund C, Brose N (2004). Calmodulin and Munc13 form a Ca2+ sensor/effector complex that controls short-term synaptic plasticity. Cell 118, 389–401.
Keerthikumar S, Chisanga D, Ariyaratne D, Al Saffar H, Anand S, Zhao K, Samuel M, Pathan M, Jois M, Chilamkurti N, *et al.* (2016). ExoCarta: a web-based compendium of exosomal cargo. J Mol Biol 428, 688–692.
Koch H, Hofmann K, Brose N (2000). Definition of Munc13-homology-domains and characterization of a novel ubiquitously expressed Munc13 isoform. Biochem J 349, 247–253.
Lacy P, Stow JL (2011). Cytokine release from innate immune cells: association with diverse membrane trafficking pathways. Blood 118, 9–18.
Lawson D, Raff MC, Gomperts B, Fewtrell C, Gilula NB (1977). Molecular events during membrane fusion. A study of exocytosis in rat peritoneal mast cells. J Cell Biol 72, 242–259.
Lee RJ, Oliver JM (1995). Roles for Ca2+ stores release and two Ca2+ influx pathways in the Fc epsilon R1-activated Ca2+ responses of RBL-2H3 mast cells. Mol Biol Cell 6, 825–839.
Lin P, Gilfillan AM (1992). The role of calcium and protein kinase C in the IgE-dependent activation of phosphatidylcholine-specific phospholipase D in a rat mast (RBL 2H3) cell line. Eur J Biochem 207, 163–168.
Lippert U, Ferrari DM, Jahn R (2007). Endobrevin/VAMP8 mediates exocytotic release of hexosaminidase from rat basophilic leukaemia cells. FEBS Lett 581, 3479–3484.
Lipstein N, Schaks S, Dimova K, Kalkhof S, Ihling C, Kolbel K, Ashery U, Rhee J, Brose N, Sinz A, Jahn O (2012). Nonconserved Ca(2+)/calmodulin binding sites in Munc13s differentially control synaptic short-term plasticity. Mol Cell Biol 32, 4628–4641.
Lollike K, Lindau M, Calafat J, Borregaard N (2002). Compound exocytosis of granules in human neutrophils. J Leukoc Biol 71, 973–980.
Lorentz A, Baumann A, Vitte J, Blank U (2012). The SNARE machinery in mast cell secretion. J Immunol 3, 143.
Luzio JP, Hackmann Y, Dieckmann NM, Griffiths GM (2014). The biogenesis of lysosomes and lysosome-related organelles. Cold Spring Harb Perspect Biol 6, a016840.
Luzio JP, Parkinson MD, Gray SR, Bright NA (2009). The delivery of endocytosed cargo to lysosomes. Biochem Soc Trans 37, 1019–1021.
Ma C, Li W, Xu Y, Rizo J (2011). Munc13 mediates the transition from the closed syntaxin-Munc18 complex to the SNARE complex. Nat Struct Mol Biol 18, 542–549.
Man KN, Imig C, Walter AM, Pinheiro PS, Stevens DR, Rettig J, Sorensen JB, Cooper BH, Brose N, Wojcik SM (2015). Identification of a Munc13-sensitive step in chromaffin cell large dense-core vesicle exocytosis. Elife 4, e10635.
Manderson AP, Kay JG, Hammond LA, Brown DL, Stow JL (2007). Subcompartments of the macrophage recycling endosome direct the differential secretion of IL-6 and TNFalpha. J Cell Biol 178, 57–69.

Marshall MR, Pattu V, Halimani M, Maier-Peuschel M, Muller ML, Becherer U, Hong W, Hoth M, Tschernig T, Bryceson YT, Rettig J (2015). VAMP8-dependent fusion of recycling endosomes with the plasma membrane facilitates T lymphocyte cytotoxicity. J Cell Biol 210, 135–151.
Mascia L, Langosch D (2007). Evidence that late-endosomal SNARE multimerization complex is promoted by transmembrane segments. Biochim Biophys Acta 1768, 457–466.
Masuda ES, Luo Y, Young C, Shen M, Rossi AB, Huang BC, Yu S, Bennett MK, Payan DG, Scheller RH (2000). Rab37 is a novel mast cell specific GTPase localized to secretory granules. FEBS Lett 470, 61–64.
McDonald K, Schwarz H, Muller-Reichert T, Webb R, Buser C, Morphew M (2010). "Tips and tricks" for high-pressure freezing of model systems. Methods Cell Biol 96, 671–693.
Menager MM, Menasche G, Romao M, Knapnougel P, Ho CH, Garfa M, Raposo G, Feldmann J, Fischer A, de Saint Basile G (2007). Secretory cytotoxic granule maturation and exocytosis require the effector protein hMunc13-4. Nat Immunol 8, 257–267.
Murk JL, Posthuma G, Koster AJ, Geuze HJ, Verkleij AJ, Kleijmeer MJ, Humbel BM (2003). Influence of aldehyde fixation on the morphology of endosomes and lysosomes: quantitative analysis and electron tomography. J Microsc 212, 81–90.
Neeft M, Wieffer M, de Jong AS, Negroiu G, Metz CH, van Loon A, Griffith J, Krijgsveld J, Wulffraat N, Koch H, *et al.* (2005). Munc13-4 is an effector of rab27a and controls secretion of lysosomes in hematopoietic cells. Mol Biol Cell 16, 731–741.
Nemoto T, Kimura R, Ito K, Tachikawa A, Miyashita Y, Iino M, Kasai H (2001). Sequential-replenishment mechanism of exocytosis in pancreatic acini. Nat Cell Biol 3, 253–258.
Pang ZP, Sudhof TC (2010). Cell biology of Ca2+-triggered exocytosis. Curr Opin Cell Biol 22, 496–505.
Paumet F, Le Mao J, Martin S, Galli T, David B, Blank U, Roa M (2000). Soluble NSF attachment protein receptors (SNAREs) in RBL-2H3 mast cells: functional role of syntaxin 4 in exocytosis and identification of a vesicle-associated membrane protein 8-containing secretory compartment. J Immunol 164, 5850–5857.
Pei J, Ma C, Rizo J, Grishin NV (2009). Remote homology between Munc13 MUN domain and vesicle tethering complexes. J Mol Biol 391, 509–517.
Peters C, Mayer A (1998). Ca2+/calmodulin signals the completion of docking and triggers a late step of vacuole fusion. Nature 396, 575–580.
Pfaffl MW (2001). A new mathematical model for relative quantification in real-time RT-PCR. Nucleic Acids Res 29, e45.
Pickett JA, Edwardson JM (2006). Compound exocytosis: mechanisms and functional significance. Traffic 7, 109–116.
Pivot-Pajot C, Varoqueaux F, de Saint Basile G, Bourgoin SG (2008). Munc13-4 regulates granule secretion in human neutrophils. J Immunol 180, 6786–6797.
Pryor PR, Mullock BM, Bright NA, Gray SR, Luzio JP (2000). The role of intraorganellar Ca(2+) in late endosome-lysosome heterotypic fusion and in the reformation of lysosomes from hybrid organelles. J Cell Biol 149, 1053–1062.
Puri N, Roche PA (2008). Mast cells possess distinct secretory granule subsets whose exocytosis is regulated by different SNARE isoforms. Proc Natl Acad Sci USA 105, 2580–2585.
Raposo G, Tenza D, Mecheri S, Peronet R, Bonnerot C, Desaymard C (1997). Accumulation of major histocompatibility complex class II molecules in mast cell secretory granules and their release upon degranulation. Mol Biol Cell 8, 2631–2645.
Ren Q, Barber HK, Crawford GL, Karim ZA, Zhao C, Choi W, Wang CC, Hong W, Whiteheart SW (2007). Endobrevin/VAMP-8 is the primary v-SNARE for the platelet release reaction. Mol Biol Cell 18, 24–33.
Ren Q, Wimmer C, Chicka MC, Ye S, Ren Y, Hughson FM, Whiteheart SW (2010). Munc13-4 is a limiting factor in the pathway required for platelet granule release and hemostasis. Blood 116, 869–877.
Savina A, Fader CM, Damiani MT, Colombo MI (2005). Rab11 promotes docking and fusion of multivesicular bodies in a calcium-dependent manner. Traffic 6, 131–143.
Seldin DC, Adelman S, Austen KF, Stevens RL, Hein A, Caulfield JP, Woodbury RG (1985). Homology of the rat basophilic leukemia cell and the rat mucosal mast cell. Proc Natl Acad Sci USA 82, 3871–3875.
Shen J, Tareste DC, Paumet F, Rothman JE, Melia TJ (2007). Selective activation of cognate SNAREpins by Sec 1/Munc18 proteins. Cell 128, 183–195.
Shin OH, Lu J, Rhee JS, Tomchick DR, Pang ZP, Wojcik SM, Camacho-Perez M, Brose N, Machius M, Rizo J, *et al.* (2010). Munc13 C2B domain is an activity-dependent Ca2+ regulator of synaptic exocytosis. Nat Struct Mol Biol 17, 280–288.
Shirakawa R, Higashi T, Tabuchi A, Yoshioka A, Nishioka H, Fukuda M, Kita T, Horiuchi H (2004). Munc13-4 is a GTP-Rab27-binding protein regulating dense core granule secretion in platelets. J Biol Chem 279, 10730–10737.
Singh RK, Mizuno K, Wasmeier C, Wavre-Shapton ST, Recchi C, Catz SD, Futter C, Tolmachova T, Hume AN, Seabra MC (2013). Distinct and opposing roles for Rab27a/Mlph/MyoVa and Rab27b/Munc13-4 in mast cell secretion. FEBS J 280, 892–903.
Stow JL, Murray RZ (2013). Intracellular trafficking and secretion of inflammatory cytokines. Cytokine Growth Factor Rev 24, 227–239.
Sudhof TC (2012). Calcium control of neurotransmitter release. Cold Spring Harb Perspect Biol 4, a011353.
Sudhof TC, Rothman JE (2009). Membrane fusion: grappling with SNARE and SM proteins. Science 323, 474–477.
Takahashi S, Kubo K, Waguri S, Yabashi A, Shin HW, Katoh Y, Nakayama K (2012). Rab11 regulates exocytosis of recycling vesicles at the plasma membrane. J Cell Sci 125, 4049–4057.
Thorn P, Gaisano H (2012). Molecular control of compound exocytosis: a key role for VAMP8. Commun Integr Biol 5, 61–63.
Tiwari N, Wang CC, Brochetta C, Ke G, Vita F, Qi Z, Rivera J, Soranzo MR, Zabucchi G, Hong W, Blank U (2008). VAMP-8 segregates mast cell-preformed mediator exocytosis from cytokine trafficking pathways. Blood 111, 3665–3674.
Valentijn KM, van Driel LF, Mourik MJ, Hendriks GJ, Arends TJ, Koster AJ, Valentijn JA (2010). Multigranular exocytosis of Weibel-Palade bodies in vascular endothelial cells. Blood 116, 1807–1816.
van den Hoff MJ, Moorman AF, Lamers WH (1992). Electroporation in 'intracellular' buffer increases cell survival. Nucleic Acids Res 20, 2902.
van der Sluijs P, Zibouche M, van Kerkhof P (2013). Late steps in secretory lysosome exocytosis in cytotoxic lymphocytes. J Immunol 4, 359.
Vergarajauregui S, Martina JA, Puertollano R (2009). Identification of the penta-EF-hand protein ALG-2 as a Ca2+-dependent interactor of mucolipin-1. J Biol Chem 284, 36357–36366.
Vincent-Schneider H, Thery C, Mazzeo D, Tenza D, Raposo G, Bonnerot C (2001). Secretory granules of mast cells accumulate mature and immature MHC class II molecules. J Cell Sci 114, 323–334.
Wandinger-Ness A, Zerial M (2014). Rab proteins and the compartmentalization of the endosomal system. Cold Spring Harb Perspect Biol 6, a022616.
Weber T, Zemelman BV, McNew JA, Westermann B, Gmachl M, Parlati F, Sollner TH, Rothman JE (1998). SNAREpins: minimal machinery for membrane fusion. Cell 92, 759–772.
Wesolowski J, Paumet F (2014). Escherichia coli exposure inhibits exocytic SNARE-mediated membrane fusion in mast cells. Traffic 15, 516–530.
Wood SM, Meeths M, Chiang SC, Bechensteen AG, Boelens JJ, Heilmann C, Horiuchi H, Rosthoj S, Rutynowska O, Winiarski J, *et al.* (2009). Different NK cell-activating receptors preferentially recruit Rab27a or Munc13–4 to perforin-containing granules for cytotoxicity. Blood 114, 4117–4127.
Woska JR Jr, Gillespie ME (2011). Small-interfering RNA-mediated identification and regulation of the ternary SNARE complex mediating RBL-2H3 mast cell degranulation. Scand J Immunol 73, 8–17.
Yao J, Gaffaney JD, Kwon SE, Chapman ER (2011). Doc2 is a Ca2+ sensor required for asynchronous neurotransmitter release. Cell 147, 666–677.
Yu H, Rathore SS, Lopez JA, Davis EM, James DE, Martin JL, Shen J (2013). Comparative studies of Munc18c and Munc18-1 reveal conserved and divergent mechanisms of Sec 1/Munc18 proteins. Proc Natl Acad Sci USA 110, E3271–E3280.
Yu IM, Hughson FM (2010). Tethering factors as organizers of intracellular vesicular traffic. Annu Rev Cell Dev Biol 26, 137–156.
Zenisek D, Steyer JA, Feldman ME, Almers W (2002). A membrane marker leaves synaptic vesicles in milliseconds after exocytosis in retinal bipolar cells. Neuron 35, 1085–1097.
Zografou S, Basagiannis D, Papafotika A, Shirakawa R, Horiuchi H, Auerbach D, Fukuda M, Christoforidis S (2012). A complete Rab screening reveals novel insights in Weibel-Palade body exocytosis. J Cell Sci 125, 4780–4790.